# Global air quality change during COVID-19: a synthetic result of human activities and meteorology

**Qianqian Yang[1,*], Bin Wang[1,*], Yuan Wang[1,*], Qiangqiang Yuan[1,*], Caiyi Jin[1], Jiwen Wang[1], Shuwen Li[1], Muyu Li[1], Tongwen Li[2,†], Song Liu[3], Huanfeng Shen[2], Liangpei Zhang[4]**

[1] School of Geodesy and Geomatics, Wuhan University, Wuhan, China.

[2] School of Resource and Environmental Sciences, Wuhan University, Wuhan, China.

[3] Deutsches Zentrum für Luft- und Raumfahrt (DLR), Institut für Methodik der Fernerkundung (IMF), Oberpfaffenhofen, Germany

[4] State Key Laboratory of Information Engineering in Surveying, Mapping and Remote Sensing, Wuhan University, Wuhan, China.

Corresponding author: Qiangqiang Yuan (qqyuan@sgg.whu.edu.cn); Huanfeng Shen (shenhf@whu.edu.cn); Liangpei Zhang (zlp62@whu.edu.cn).

[*]These authors contributed equally: Qianqian Yang, Bin Wang, Yuan Wang, Qiangqiang Yuan.

†Present address: School of Geospatial Engineering and Science, Sun Yat-Sen University, Guangzhou, China

## Abstract

In recent months, coronavirus disease 2019 (COVID-19) has been spreading around the globe, and this has led to a rare reduction in human activities. In such a background, data from ground-based environmental stations, satellites, and reanalysis materials are utilized to conduct a comprehensive analysis of the air quality changes during the COVID-19 outbreak at the global scale. The results showed that under the impact of the COVID-19 outbreak, a significant decrease in particulate matter ($PM_x$) and nitrogen dioxide ($NO_2$) occurred in more than 40% of the world's land area, with $NO_2$ decreasing by approximately 30% and $PM_x$ decreasing approximately 20%. In addition, the mobility, meteorological factors, and the response speed to COVID-19 outbreaks in cities were examined, and it was further found that in quick-response cities, lockdowns produced a sharp decline in mobility in a short time. This had a large impact on air quality. In contrast, in slow-response cities, declines in mobility occurred beginning with the confirmation of the first COVID-19 case (FCC) and dropped gradually for a relatively long period. The impact of the FCC, lockdowns, and meteorological factors on air quality can be comparable.



**Keywords:** Air quality, COVID-19, Lockdown, First case confirmation


## Introduction

During the past several decades, worldwide monitoring has provided concrete evidence that human activities, such as fossil fuel combustion (vehicles and factories), industrial production, construction activities, biomass burning, and changes in land use, are causing serious pollution problems in the atmosphere[1,2]. Air pollution is a major environmental risk to human health[3,4]. According to a report by the World Health Organization (WHO), nearly 91% of the world's population lives in places where the air quality levels exceed WHO limits, and ambient air pollution accounts for an estimated 4.2 million deaths per year[5]. With air pollution exerting heavy pressure on the environment, scientists around the world have conducted a large number of studies that explore how to reduce air pollution by making human activities cleaner and greener[6]. However,

there has seldom been a chance to directly observe how such changes will affect the global air quality.

The coronavirus disease 2019 (COVID-19)[7–9], which has had successive outbreaks in cities around the world[10-12], has caused unprecedented suffering[13-16]. As of May 23, 2020, the COVID-19 pandemic has caused more than 5.2 million infections and 340,477 deaths in the world[17]. People around the world have started to change their usual lifestyles to reduce the risk of infection, and countries and regions have begun to adopt various restriction measures to slow down the spread of the novel coronavirus[18,19]. People have been staying at home, cars have been idle in garages, planes have been parked in parking aprons, and some factories have been forced to close. Hence, there has been a rare large-scale slowdown of human activities all over the world. How the global air quality will change under such a situation remains an interesting question[20-22].

Currently, there are a number of studies researching the impact of the lockdowns on air quality changes[23–34]. While most of the studies are either confined to local regions[23–27] or certain types of air pollutants[27–30], there are some studies analyzing the air quality changes at the global scale and from a synthetic perspective[32–34]. However, there are still several limitations of these global studies. First, the current studies have concentrated on the impact of the lockdowns on air quality. COVID-19 affects human activities not only through lockdowns, but also in other aspects, such as the confirmation of the first COVID-19 case (FCC). The news of the first case confirmation may worry some residents and reduce their activities. Therefore, the impact of FCC on air quality should also be considered and evaluated. Second, most of the current studies have analyzed air quality changes during the COVID-19 period by simply calculating the differentials during a short period, which can be direct and intuitive, but it also could contain large uncertainties. Multiple time series analysis methods should be explored and adopted to obtain a more reliable conclusion. Finally, a combined analysis of air quality changes and mobility and meteorological changes is still lacking. Hence, a

comprehensive understanding of air quality changes during the COVID-19 outbreak at the global scale is still urgently required.

In this study, the air quality changes during the time since the COVID-19 outbreak began are investigated at the global scale. In addition, the impacts of the FCCs and lockdowns on air quality are investigated using satellite products, reanalysis data, and station measurements, and these data are analyzed in relationship to mobility changes and meteorology variations. A workflow schematic of this study is shown in Figure S1. For more details about the methods and materials, please refer to the experimental procedures and supplemental experimental procedures.

# Results

## Global air quality changes during COVID-19

The variation trends of global pollutants anomalies (methods and materials) detected using the Mann-Kendall (MK) test are depicted in Figure 1. The anomalies of $PM_{2.5}$, $PM_{10}$, and $NO_2$ significantly declined in general, while the other pollutants showed an uptrend or insignificant trend. Specifically, the percentages of areas showing significant downtrends (uptrends) during the COVID-19 epidemic were 42.32% (1.49%), 40.32% (1.21%), and 45.26% (9.52%) for the $PM_{2.5}$, $PM_{10}$, and $NO_2$ anomalies, respectively. This result is consistent with the conclusion of Venter et al.[32], although they researched the global change in $PM_{2.5}$, $O_3$, and $NO_2$ primarily based on ground station data. However, for the $O_3$, $SO_2$ and CO anomalies, the percentages were 30.45% (15.88%), 23.15% (12.68%), and 30.15% (16.07%), respectively. The spatial distribution of the regions where air quality improved varied with the pollutant types. Regions where $PM_{2.5}$ declined significantly were primarily located in the northern hemisphere and eastern Australia. The spatial distribution of the $PM_{10}$ variation trend was similar to that of $PM_{2.5}$ in most areas. However, an exception occurred in a small region of the northern Qinghai-Tibet Plateau, which is on the edge of the Taklamakan Desert. The v-component of wind (VWS) remained negative in the northern Qinghai-Tibet Plateau from January 2020 to March 2020 (Figure S2), and the anomalies of the VWS were also negative

(Figure 2), which suggested that a southern wind was prevailing and stronger than in previous years in this area. Therefore, affected by wind, the particulate matter was transported from the desert to the south and accumulated at the northern Qinghai-Tibet Plateau because of the topography. $PM_{10}$ accounted for the majority of pollution in the desert[35], so the impact on $PM_{2.5}$ was not as significant as $PM_{10}$, so the variation trends of $PM_{2.5}$ and $PM_{10}$ were different. $NO_2$ anomalies declined in most areas except for near the Arctic Circle. $O_3$ anomalies decreased significantly in the U.S., Canada, and northern Africa, but they increased in regions around the equator, possibly because of the stronger solar radiation and higher temperatures there, which can promote photochemical reactions and thus produce more $O_3$[36]. However, anomalies of $SO_2$ and CO showed increases or nonsignificant trends across the world. In addition, it is worth noting that the positive trends of four gas pollutants in the polar region (Figure 1C-F) might be inaccurate due to the great number of missing values here, which does not affect the discovery and conclusion for other areas. To demonstrate the detailed variations in air quality and their relationship with human activities, China, Europe, the Contiguous United States (CONUS), and Brazil (Figure S3) were focused on, where COVID-19 was the most prevalent[12,16,37].

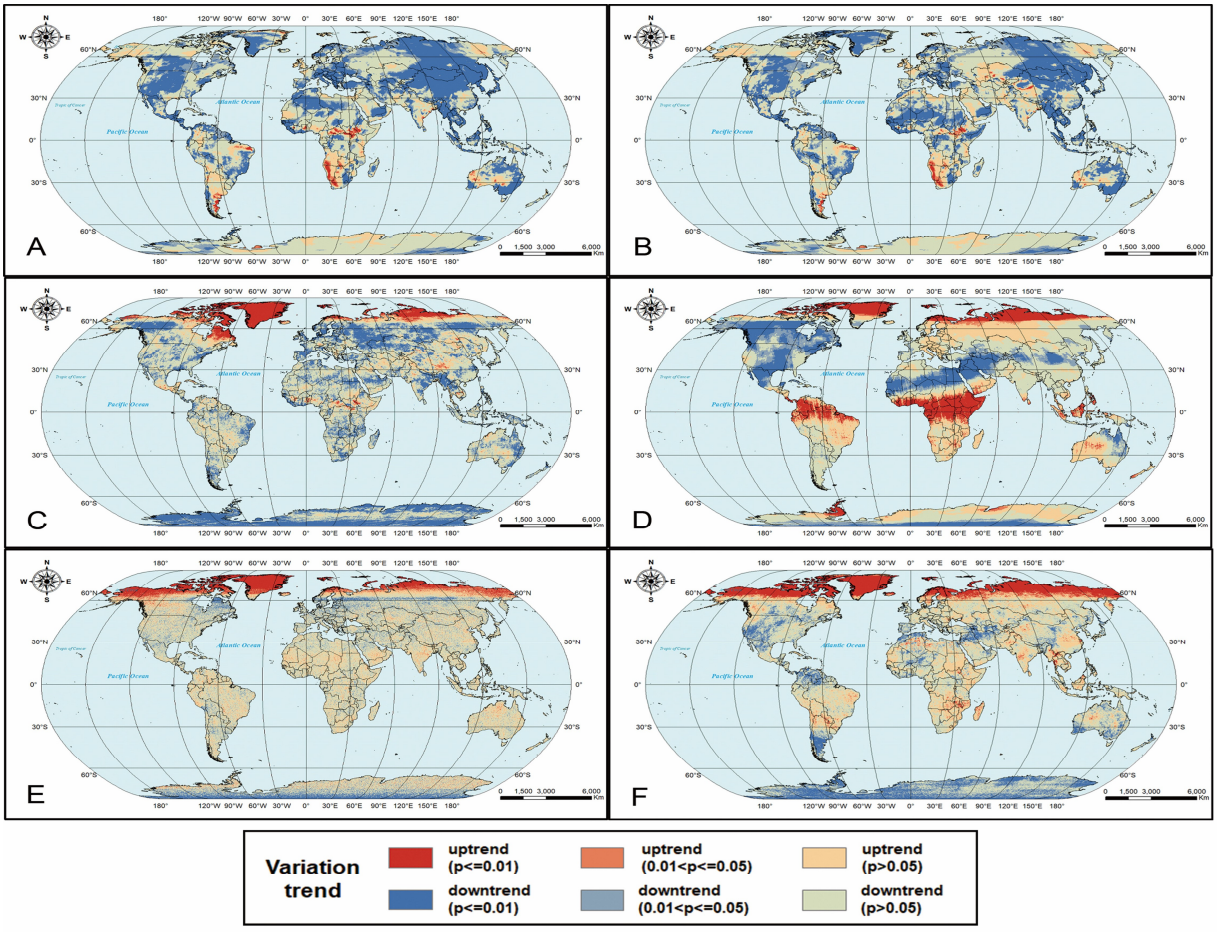


**Figure 1.** Variation trends and the significance of six pollutant anomalies. The trends and significances of all of the pollutants were calculated using the MK test. A-F represent the global distribution of the results of anomalies in $PM_{2.5}$, $PM_{10}$, $NO_2$, $O_3$, $SO_2$, and CO, respectively.

$PM_{2.5}$ and $PM_{10}$ ($PM_x$) anomalies decreased significantly in northwestern China, central and northeastern CONUS, and most parts in Europe and Brazil. The $PM_x$ anomalies remained negative in most regions of China during COVID-19. While in Europe, the signs of $PM_{2.5}$ anomalies did not display a uniform pattern prior to week four, and then the values remained negative in most areas until week 12 (Figure S4). Although there were no compulsory measures declared by the local governments then, it was inferred that people were likely to spontaneously reduce their outing activities after the COVID-19 pandemic began to be prevalent. Therefore, this caused a decline in $PM_{2.5}$. The trend in the anomalies of $PM_{10}$ was similar to $PM_{2.5}$ in most areas of Europe, except the Southwest portion (Figure S5). In the northeastern CONUS, the anomalies of $PM_{2.5}$ were negative

121 in week 11. This was close to the time (March 19, 2020) that the number of CONUS cases exceeded
122 10,000, and 40% of them were in New York State. The spatiotemporal pattern of the anomalies of
123 PMx and CO in Brazil were similar. Both of these pollutants decreased in most of the area, but they
124 were unexpectedly increased in the eastern coastal area and in the countries southwest of Brazil.
125 Figure 2C shows that the zonal wind (UWS, positive represent eastward wind) in the eastern coastal
126 areas of Brazil showed positive anomalies. Considering that westward wind prevails in eastern
127 Brazil from January to March, the positive UWS anomalies could have indicated a decrease in the
128 westward wind speed, which were likely to lead to an accumulation of pollutants. Therefore, the
129 anomalies of $PM_x$ concentration showed an uptrend in the east with time. For other regions in Brazil
130 where the meteorological data did not significantly change, the concentration of $PM_x$ still declined
131 under the impact of the COVID-19 lockdown. As for the $PM_x$ and CO increases in the countries
132 southwest of Brazil, it was inferred this might have been a result of increased wildfires. These areas
133 witnessed an increase in wildfire frequency in 2020 compared with 2019, especially since March
134 (Figure S6), thus leading to an increase in $PM_x$ and CO.

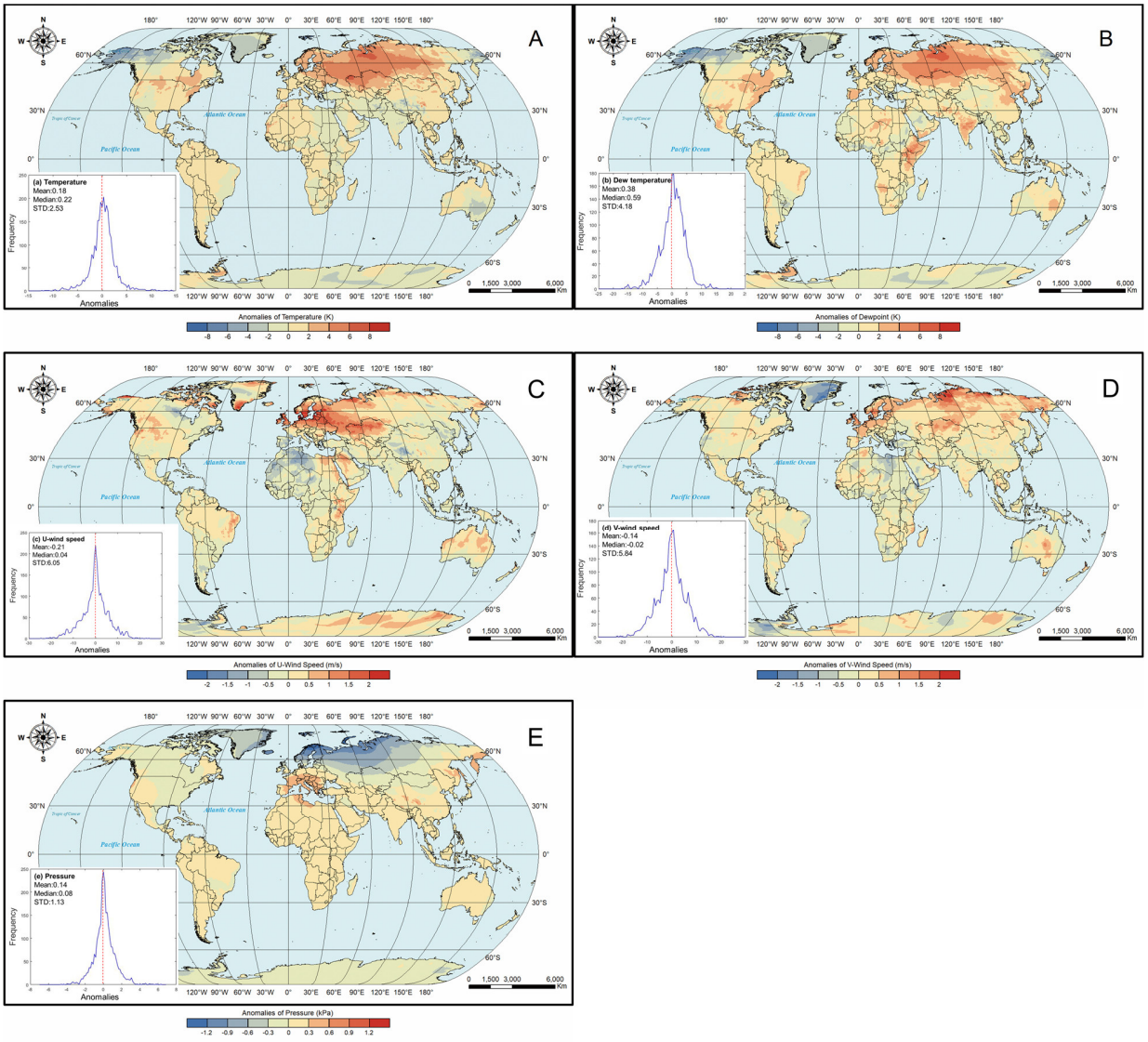


**Figure 2.** The average anomalies from January to April 2020 of six meteorological factors. The baseline for the anomalies is the average meteorological conditions for the same period during 2017–2019. A-F represent the anomalies for temperature (TEM), dewpoint temperature (DEW), zonal wind (UWS), meridional wind (VWS), and pressure (PS), respectively. The probability distribution plot in the bottom left corner of each subfigure shows the frequency distribution of the meteorological anomalies in the 26 studied cities.

For $NO_2$, the anomalies primarily had a significant downward trend in central and northern China (Figures S3 and S7), which was most probably related to the restrictive measures issued by the government[38]. Specifically, the anomalies experienced a -129% fractional change after

lockdown started, which was consistent with the conclusion of Le et al. They calculated a change percentage based on data from 2019 to 2020 of -71.9%[39]. The anomalies of $NO_2$ typically fluctuated in central and eastern China prior to the outbreak of COVID-19 (Figure S7). During the lockdown period which started on January 23, 2020 in Wuhan, the $NO_2$ anomalies remained negative in most areas of central and eastern China until week 12. The next week, due to work resumptions, the anomalies of $NO_2$ turned positive. Compared to China, the timing of the changes in the $NO_2$ anomalies in Europe showed a certain delay due to the difference in the COVID-19 outbreak time (Figure S7). The anomalies of $NO_2$ turned negative in most areas after week 11 when the local governments declared their restrictions to deal with the COVID-19 epidemic. In the eastern CONUS, the values turned negative in week eight. Although the values fluctuated in week 12 in some areas, they remained negative in areas with severe epidemic, such as New York. The anomalies in $NO_2$ showed a significant downtrend in urban areas in east Brazil. However, the concentration of $NO_2$ in Brazil were less serious than in the other three places, so the weekly variations in the anomalies (Figure S7) were unobvious from a satellite perspective relative to other regions.

For the other three pollutants, the variation trends were not as significant as $PM_x$ and $NO_2$, but the turning points of the time series were related to the COVID-19 lockdown time. The turning point of the $O_3$ anomalies in the CONUS was observed at the $11^{th}$ week, and the anomalies of $SO_2$ and CO also turned at approximately week 12, all close to the lockdown time in the CONUS. The turning point of the $SO_2$ anomalies in Europe was week nine, which was near to most of the European countries lockdown times. As demonstrated above, the satellite and reanalysis data showed that the global air quality significantly improved during COVID-19, and the turning points of pollutants variations were closely related to lockdown times.

**Ground-based air quality changes in typical cities**

Satellite and reanalysis data can monitor air quality changes over a large extent with relatively continuous spatial coverage. However, the results may not be able to exactly reflect near-surface pollution variations. Therefore, 26 typical cities were selected and ground-based monitoring data were utilized for further analysis. There were different lockdown periods in different countries and cities, thus a study period was chosen that covered most of the important time nodes in these cities (e.g., the FCC and lockdown). Specifically, the study period was from January 1, 2020 to April 24, 2020, and the distribution of cities and the time nodes of each are shown in Figure S8. The cities were divided into two groups according to the time difference between the FCC and the lockdown. Cities with a time difference of fewer than 50 days (for more information about the determination of the threshold, please refer to Figure S9) were defined as quick-response cities (11 out of 26 cities). The others were defined as slow-response cities (15 out of 26 cities). For each city, the change curves of the daily air quality index (AQI, for more information, please refer to experimental procedures section) during the study period are displayed in Figure S10, and the change percentage since the FCC or lockdown are shown in Figure 3 and Table S1. The results indicated that for $PM_{2.5}$, $PM_{10}$, and $NO_2$, most of the cities showed an obvious decreasing trend, which agrees with many of the current studies[25,26,28-32]. One of the common sources of $PM_{2.5}$, $PM_{10,}$ and $NO_2$ is vehicle exhaust emissions. The transportation density during the COVID-19 outbreak largely decreased (Figure S11), directly leading to a decline in vehicle exhaust emissions and the AQIs of $PM_{2.5}$, $PM_{10,}$ and $NO_2$. In addition, $O_3$ and CO also decreased during the study period, but in most cases, the declines were insignificant ($p>0.05$). The change in $SO_2$ was insignificant ($p>0.05$), as well for most of the cities, with an insignificant decrease prior to lockdown, and an insignificant increase after the FCC. In general, the results from the ground-based observations were similar to those of the satellite and reanalysis material.

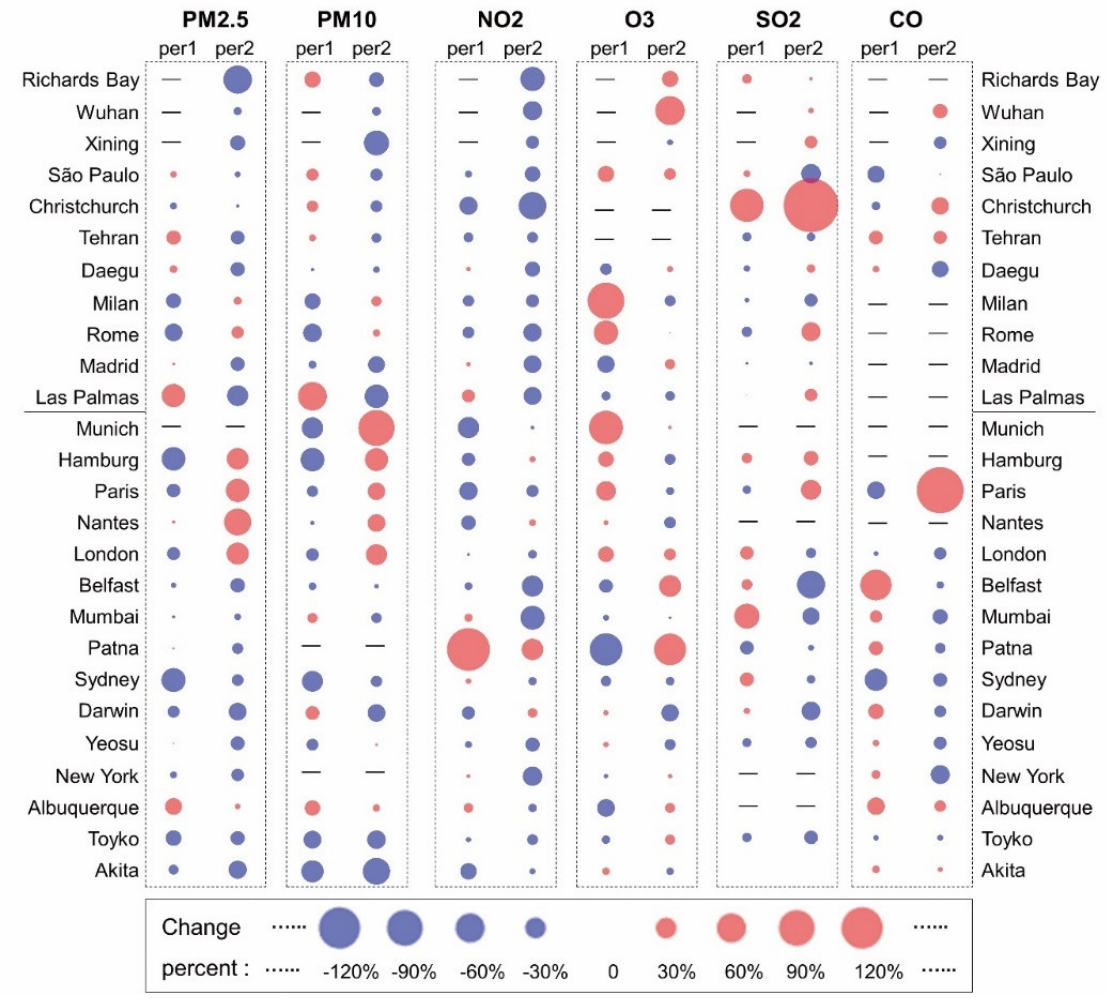


**Figure 3.** The percentage change in the AQI after FCC/lockdown (per1/per2) for six pollutants in 26 cities. The blue (red) circles indicate a decrease (increase) in the AQI, the larger the circle, the greater the AQI decrease/increase. The dash lines in the rectangles stand for missing data. Cities above the black lines are the quick-response cities and below the lines are the slow-response cities.

**Correlation between the FCC\lockdown and air quality changes**

The satellite and reanalysis data revealed the relationships between air quality changes and human activity slowdowns caused by the COVID-19 pandemic. Ground-based data were used to quantify these relationships. The time when the daily air quality anomalies began to change (referred to as the change point hereafter) was detected using a time series analysis approach. The results showed that these change points were highly correlated with the time of the FCC/lockdowns (Figure 4A and Table S2). Generally, the change point of $NO_2$ had the highest correlation with the

FCC/lockdown time, with correlation coefficients, *r*, of 0.69 ($p<0.05$) and 0.58 ($p<0.05$), respectively. $O_3$ had r of 0.56 ($p<0.05$) and 0.51 ($p<0.05$) for lockdown time and the FCC time, respectively. In addition, the change point of the $PM_{2.5}$ AQI anomalies had a high correlation with the time of the FCC ($r=0.53$, $p<0.05$), but it had a relatively low correlation ($r=0.26$, $p=0.21$) with the lockdown time. The *r* values for the other three pollutants ranged from 0.23 to 0.48.

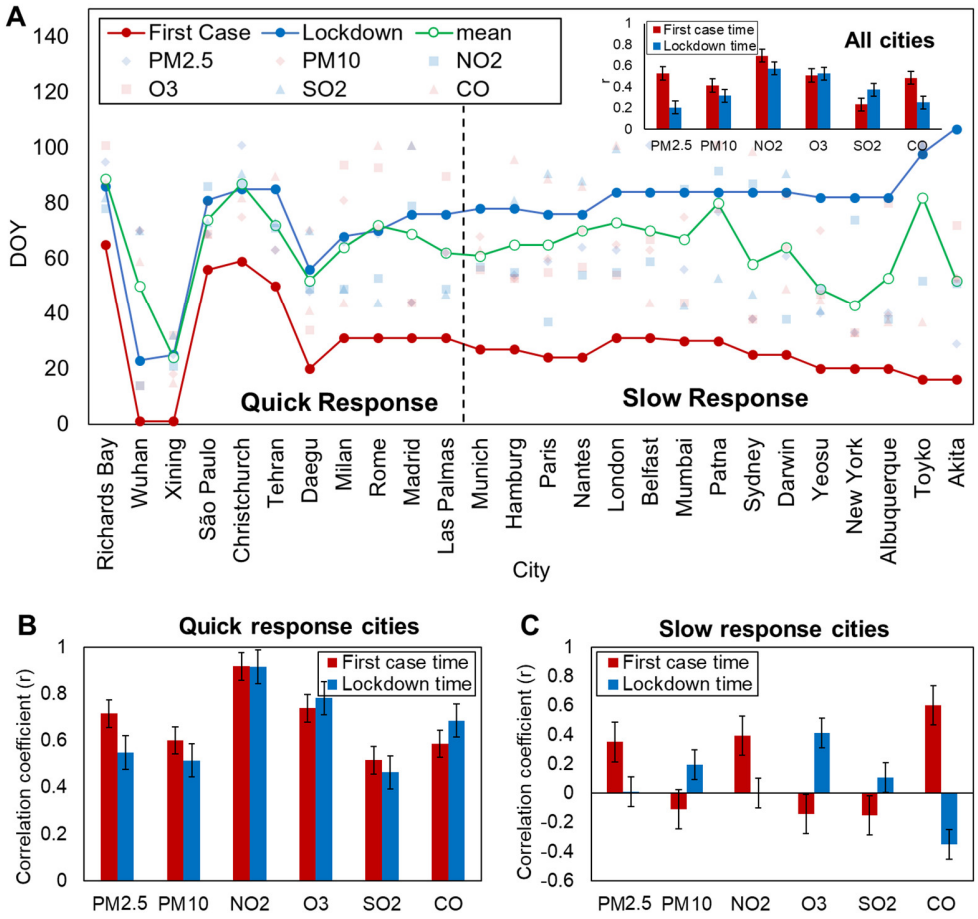


**Figure 4.** The relationship between the change point in the time series and the time of the FCC/lockdown. (A) The detected change point times and the FCC/lockdown times in the 26 cities. DOY represents the day of year. The green line is the mean times of the change points of the six pollutants. The histogram in the upright corner displays the correlation between them. (B) The correlations between the change point times and the FCC/lockdown times in the quick-response cities and (C) in the slow-response cities.

A comparison was also conducted between the quick- and slow-response cities. In the quick-response cities, the change points were very close to the lockdown time and then got closer to the FCC time in slow-response cities (Figure 4A). In addition, in the quick-response cities, the correlations between the change points and the FCC/lockdown times (*r* ranges from 0.48 to 0.92) were much higher than that in the slow-response cities (*r* ranges from -0.38 to 0.58) (Figure 4B, C). COVID-19 caused air quality changes primarily due to alterations in human activities. When a city made a quick response to the COVID-19 pandemic, social activities and human behaviors changed drastically in a short time due to the restrictions. Therefore, changes in human activities caused by the lockdown became the dominant factor affecting air quality, which explains the high consistency between the change points in air quality and the lockdown times. In contrast, in the slow-response cities, human activities changed gradually over a long period of time, urged either by the fear of being infected when the first case appeared or due to government restrictions. During this period, the influencing factors of air quality were not dominated by lockdown anymore, and the impact of lockdown, the FCC, and meteorological factors could be comparable. This could be the reason for the poor correlations between air quality change points and the lockdown/FCC times in the slow-response cities.

**Quantification of the impact of the FCC and lockdowns on air quality**

For a quantitative description of how much the air quality had changed under the impact of the FCCs and lockdowns, the change percent of the AQI during the different periods were calculated and summarized for several typical regions (Table S3). The results showed that both the FCCs and lockdowns brought a large reduction in $NO_2$ in most cities, with lockdowns typically bringing larger changes (22% [95% confidence interval:14%, 30%]) than the FCCs (9% [3%, 16%]). However, in Europe, the changes in $NO_2$ caused by the FCCs and lockdowns were similar (16% [7%, 26%] for the FCC and 16% [5%, 26%] for the lockdowns). An exception occurred in Patna, India, where the AQI anomalies of $NO_2$ increased greatly after the FCC (180%) and the lockdown

(46%). Patna was a heavily-polluted[40,41] and lightly-infected city. Transportation data showed that mobility in Patna did not decrease during the COVID-19 outbreak (Figure 5A), while in Mumbai, India, mobility decreased significantly (Figure 5B). In addition, $O_3$ in Patna decreased 103.96% since the FCC (Figure 3, Table S1), which was the largest among all of the 26 cities. Previous studies had shown that an inverse relationship existed between $O_3$ and $NO_2$[42-44], which was also detected by the analysis results of this study, as shown in Figure S10 (the variation trends of $O_3$ and $NO_2$ were nearly opposite). Based on the above points, it was inferred that the ongoing human activities and the interactions between air pollutants caused the increase in $NO_2$ in Patna.

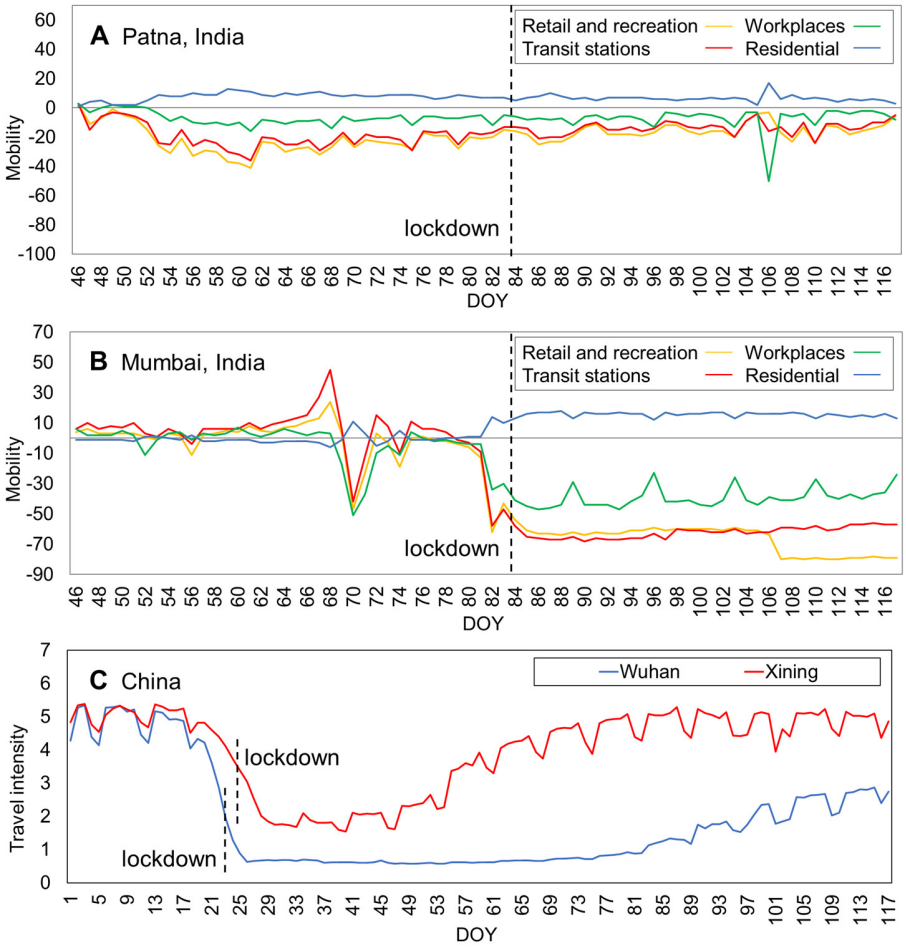


**Figure 5.** Daily variations in mobility and travel intensity in four typical cities. (A, B) The mobility variations in Patna and Mumbai, India. (C) The travel intensity variations in Wuhan and Xining, China.

253 Additionally, $PM_x$ also decreased by a large amount after the FCCs and lockdowns.
254 Specifically, the lockdowns caused a decline of 24% (10%, 39%) in Asian and Africa and 12% (4%,
255 16%) in the cities of North America, South America, and Australia. In contrast, the FCCs brought
256 little changes to $PM_x$ in these regions. An interesting phenomenon appeared in cities in Europe
257 (Rome and Milan in Italy, Paris, and Nantes in France, Hamburg in Germany, and London in the
258 U.K.). $PM_x$ declined by 20% (14%, 32%) after the FCC, but increased greatly (28% [3%, 53%])
259 during the European lockdowns. The meteorological data showed that European cities experienced
260 extremely unfavorable meteorological conditions during the lockdowns (Figures S12–S13). To be
261 specific, compared with other cities, the European cities witnessed large increases in pressure and
262 dewpoint temperatures and a decrease in wind speeds since the lockdowns began (Figure 6). It can
263 be inferred that the high-humidity, high-pressure, and low-wind-speed conditions offset the
264 improvements in the $PM_x$ pollution caused by the COVID-19 lockdowns. Asian cities and other
265 cities have also experienced small declines in wind speed, but generally, the overall meteorological
266 conditions did not change significantly compared with the period prior to the lockdowns.

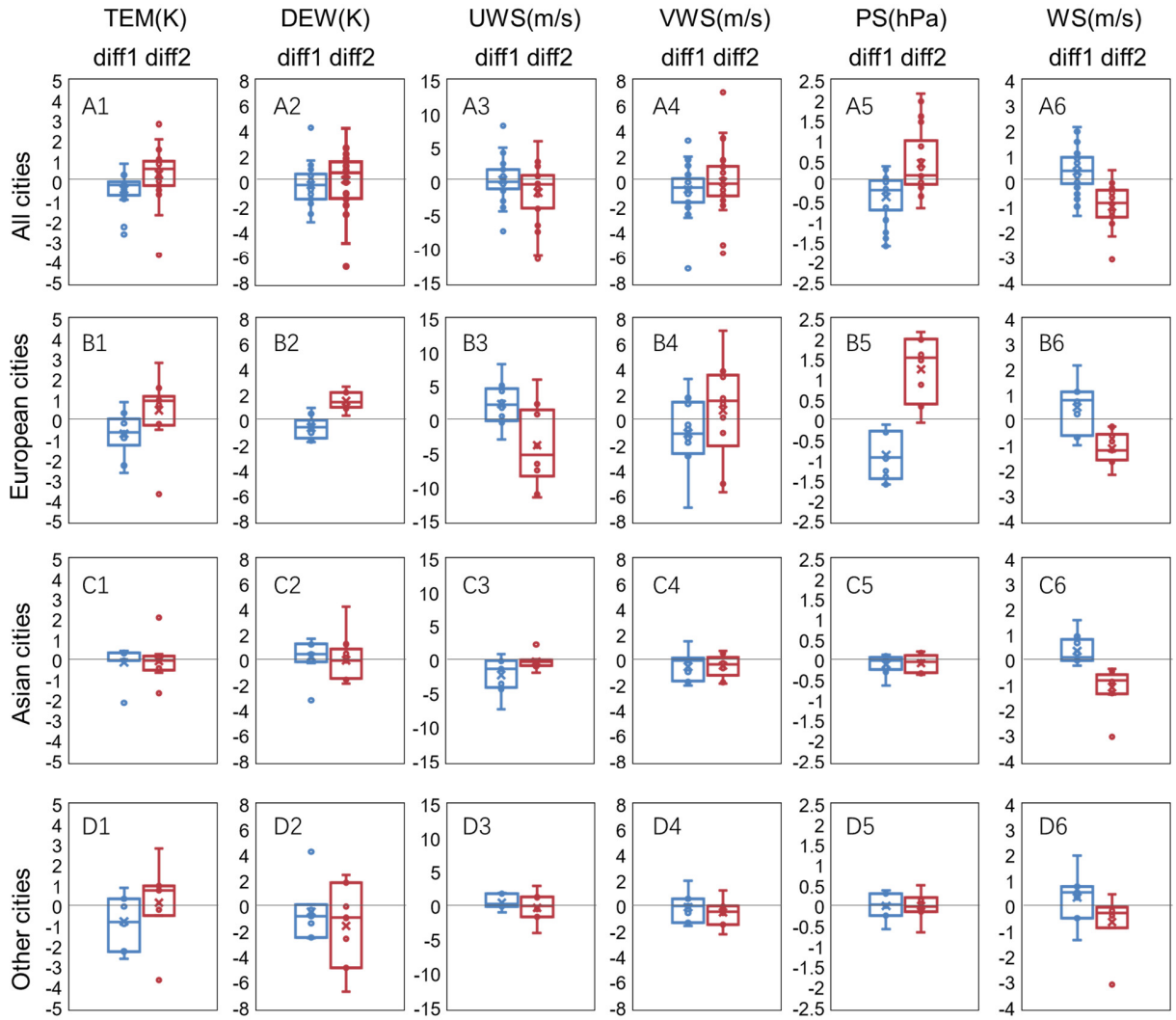


**Figure 6.** The boxplot for the changes in the meteorological anomalies after the FCC/lockdowns (diff1/diff2) in the different groups of cities. The blue box plots represent diff1, and the red represent diff2. The first five meteorological factors have the same meaning as in Figure 2. The last variable, WS, represents the composite wind speed, which was calculated from the UWS and VWS.

The changes in the other three atmospheric pollutants were not as obvious as for $NO_2$ and $PM_x$. Among them, $O_3$ showed an increase in some cities after the FCCs and lockdowns, which has been paid special attention by some researchers[39,45]. It was inferred to be a result of a nonlinear production chemistry of ozone in the atmosphere, and reduced nitrogen oxides resulted in ozone enhancement[39]. CO showed a mild increase after the FCCs and a mild decrease during lockdown in most regions. As for $SO_2$, the variation trend showed strong spatial heterogeneity.

The impact of the FCCs and lockdowns on air quality varied with cities. In the quick-response cities (the upper portion of Figure 3), the lockdowns typically caused a larger decline than the FCCs, but in the slow-response cities (the lower portion of Figure 3), the case was more complicated, and it was likely that the effect of the FCCs and lockdowns were comparable. As mentioned earlier, in some of the slow-response cities (not all), people may have already tried to avoid going out since the appearance of the first case. The changes in human activities caused by the COVID-19 pandemic happened gradually in a relatively long period of time, rather than changing sharply in a short time like in the quick-response cities. Therefore, the changes in air quality were not dominated by the lockdown, but they could have been affected by multiple factors, such as the FCCs and meteorological factors. An interesting phenomenon that can be seen in Figure 3 also demonstrates this opinion. It has been discussed that an increase in $PM_{2.5}$ and $PM_{10}$ after the lockdowns in European cities was caused by unfavorable meteorological conditions that offset the impact of the lockdowns. Then it was found that the offset effect was more obvious in the slow-response cities than in the quick-response cities. This is because the lockdowns had a larger impact on air quality in the quick-response cities than in the slow-response cities, which is consistent with the conclusion above.

**Mobility variation during COVID-19**

Finally, for a further demonstration of the above conclusions, the mobility data for different regions were utilized (Figure S11), and the contributions of the FCCs and lockdowns to the changes in mobility were calculated. The results showed similar conclusions. First, a decrease in mobility in retail and recreation places, transit stations, and workplaces was observed. Additionally, the mobility in residential areas increased during the COVID-19 outbreak (Figure S11). This result indicated a decrease in the travel frequency, which may explain the reduction in $PM_{2.5}$, $PM_{10,}$ and $NO_2$ pollution. Second, in the quick-response cities, the lockdowns contributed most to the mobility changes; however, in slow-response cities, the contribution of the FCCs to mobility change

increased compared with the quick-response cities (Figure 7). This may explain why the lockdowns had a larger impact on air quality in the quick-response cities than in the slow-response cities. The consistency between the mobility changes and air quality changes also revealed the relationship between human activities and atmospheric pollution.

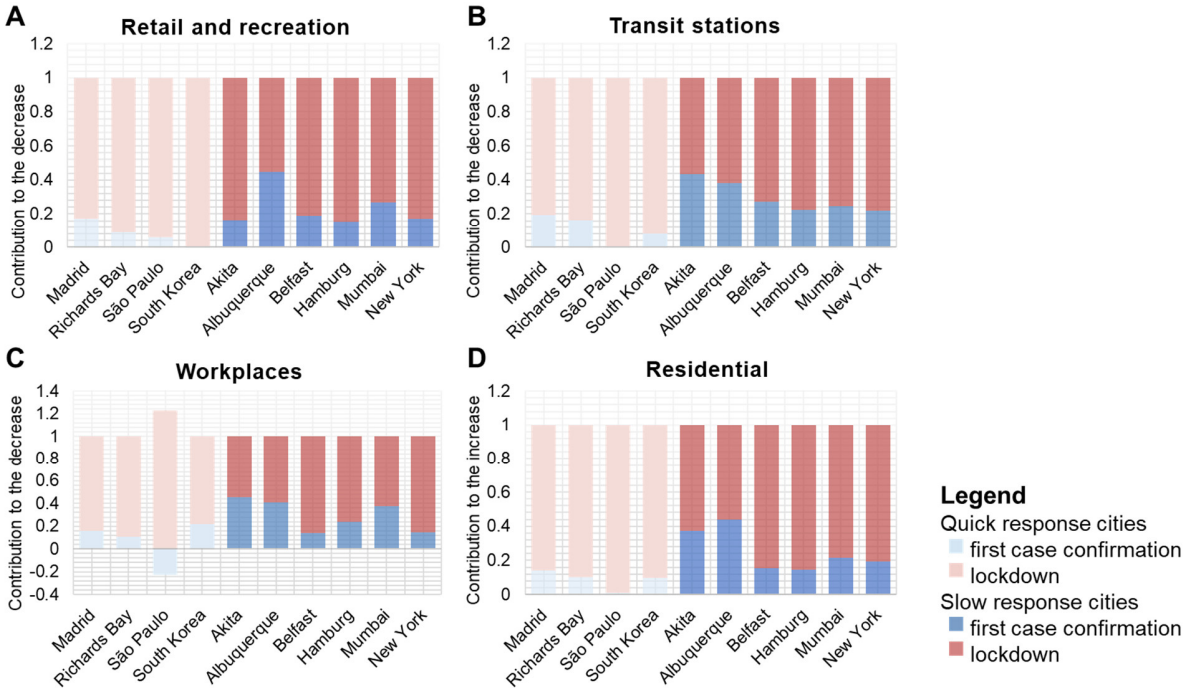


**Figure 7.** The contribution of the FCCs/lockdowns to the total mobility declines (increase for (D)) in different places. The cities represented by the light color bars are the quick-response cities, and the others are the slow-response cities. The red portions are the contributions of the lockdowns and the blue is the contribution of the FCCs.

## Discussion

### Difference in trends between the original observations and the anomalies

Most air pollutants can vary with months under the impact of meteorological conditions (for example $PM_{2.5}$ may decrease from January to April, and $O_3$ may increase from January to April in China)[46,47]. Therefore, the pollutant anomalies concentration data for 2020 were calculated using data from previous years as a baseline to remove the impact of the inner pollutant variation trends. The MK test results are shown in Figure 1. For comparison, the MK test was also conducted on the

original pollutant observations for the same time period (Figure S14). As shown, there is a clear difference between the original observations and the anomalies.

$PM_x$ increased in most areas with high latitudes in the northern hemisphere, but the $PM_x$ anomalies showed an opposite trend in northern China, the northern U.S., and areas near the Arctic Circle. However, in western Australia, $PM_x$ showed a significant downtrend in the original results, but not a significant downtrend or even an uptrend in the anomaly results. Although two kinds of results for $NO_2$ showed similar variation trends in most areas of the world, except for northern Southeast Asia and western China, the significances of the anomalies were lower than those of the original observations on the whole. The spatial distribution of the original $O_3$ observations had obvious characteristics of latitude stratification. The temperature and solar radiation in areas near the equator are higher and stronger, and this is favorable for the production of $O_3$[48]. A similar but less obvious pattern was observed in the $O_3$ anomaly results. The original $SO_2$ results showed a more significant uptrend near the equator as well. As for CO, the original observations increased significantly in most areas of the northern hemisphere. The northern hemisphere is subject to dry weather conditions from September to March of the following year, and this is the peak season for hill fires in the northern hemisphere, which will lead to rapid increases in CO concentrations[49]. However, the anomaly results displayed a totally different pattern. In most areas, CO had no significant variation, which meant that the change in CO was caused by its inner periodicity affected by meteorological conditions. As demonstrated above, the process of calculating anomalies effectively eliminated the inner variation pollution trends and improved the accuracy of this analysis.

**Impact of work resumption**

During the study period, two cities, namely, Wuhan and Xining, had ended their lockdown and started to resume work and production, which is usually accompanied by a resumption of human activities. Therefore, it will be interesting to observe the air quality changes after work

resumption. Wuhan gradually began to resume work and production in week 12. The satellite and reanalysis data showed that the $NO_2$ anomalies in the Wuhan area started to show an increasing trend after week 12. During week 13, the anomalies turned to large positive values, indicating a large increase compared with the $NO_2$ concentrations of previous years. The ground-based measurements showed similar results. Specifically, in Wuhan, the $PM_{2.5}$, $PM_{10,}$ and $NO_2$ increased by 12.85%, 15.29%, and 38.08%, respectively, after work resumption. In Xining, the work resumption led to an increase of 16.68%. 73.25%, and 7.01%, for $PM_{2.5}$, $PM_{10,}$ and $NO_2$, respectively. Apart from $PM_x$ and $NO_2$, $SO_2$ also showed an increase (39.37% for Wuhan and 11.57% for Xining), while the changes in CO and $O_3$ were mild.

The variations in transportation data in Wuhan and Xining were also analyzed (Figure 5C). The results showed that the travel intensity began to increase after February 17, 2020, when Xining started to resume work and production. In Wuhan, the case was similar, and travel intensity began to increase after March 25, 2020. The change in air quality could be closely related to the changes in transportation, which again, revealed the relationship between air pollution and human activities.

## Conclusion

Industrial development has been accused of being the primary cause of air pollution in the past several decades. The breakout of the COVID-19 pandemic has provided a special test foundation to investigate the relationship between them. In this study, multisource data were utilized to quantify the air quality changes and the impacts of COVID-19 FCCs and lockdowns on air quality changes. The results showed that the COVID-19-related human activity slowdowns resulted in the greatest reduction in $NO_2$ pollution, which dropped by approximately 30% since the COVID-19 breakout on the global scale. Then the $PM_{2.5}$ and $PM_{10}$. Most cities witnessed a percentage decline of approximately 20%, except for cities in Europe. Unfavorable meteorological conditions since the end of March in European cities offset the influence of the lockdowns, and this worsened $PM_{2.5}$ and $PM_{10}$ pollution. The changes in $O_3$, $SO_{2,}$ and CO pollution were not as obvious as for $PM_x$ and

$NO_2$, but indications of ozone enhancement and CO decreases were seen in some areas. While most current studies have focused only on the impact of lockdowns and have concluded that lockdowns are followed by air quality improvements, this study found that this was not always the case. In those cities with a relatively quick responses to the outbreak of the COVID-19 pandemic, the effect of lockdowns on air quality was typically significant, but for the slow-response cities, the effect of FCCs and meteorological parameters on air quality was found to also be significant.

Although this study has drawn numerous valuable conclusions, there are still limitations of this study. For example, the observations from TROPOMI only provided information on the total/tropospheric vertical column for the different atmospheric pollutants, which may not be greatly affected by human activities/emission sources in some regions. As a consequence, future work must first aim at generating high-accuracy global ground-level concentrations of each atmospheric pollutant by combing multiple datasets (e.g., ground-based sites and TROPOMI). Next, the generated results were employed for the analyses of air quality, which is expected to indicate more significant temporal variations related to the human activities/emission sources. Additionally, the results of this study were primarily obtained from the statistical analysis, which may be insufficient for exploring the reasons for air quality changes. Although a detailed and comprehensive investigation was conducted regarding the air quality changes during COVID-19, there are some results that were not fully explained. It is hoped that these findings can provide some interesting topics or directions for atmospheric chemistry or model simulation researchers, and taken together, our understanding of COVID-19's impact on the atmosphere can be further improved. Finally, as some studies have proposed[33,53], COVID-19 has not only had a short-run influence on the earth system, but it can also have a long-run impact. Long-term and continuous observations and analyses will be of great significance in the future.

# Resource availability

## Data and code availability

Satellite products were download from https://disc.gsfc.nasa.gov/. Reanalysis products are accessible at https://apps.ecmwf.int/datasets/data/cams-nrealtime/levtype=sfc/. Global air quality index data are accessible at https://aqicn.org/. Transportation data of China was supported by the Baidu migration dataset (https://qianxi.baidu.com), while those of other countries were provided by Google mobility reports (https://www.google.com/covid19/mobility/). For more details regarding the datasets and preprocessing, please refer to the supplemental experimental procedures section. The methods described in this article were implemented using MATLAB (R2020a). The specific datasets and codes used in this study are available from the lead contact on request.

## Materials and methods

### Time series analysis for the satellite and reanalysis data.

First, the pollutant anomalies were calculated using previous observations as a baseline to remove the impact of the inner pollutant variation trends, which has been a widely used and effective strategy found in similar studies[18,39,50-52].

$$abCon_j = Con_{j,2020} - \sum_{i=2017}^{2019} Con_{j,i}/3\,, \quad (1)$$

where *Con* means the concentration data; *j* represents the types of air pollutants, including $PM_{2.5}$, $PM_{10}$, $SO_2$, $NO_2$, $O_3$, and CO; and *i* represents the previous years, from 2017 to 2019. Negative anomalies show that the air pollution decreased in 2020 compared with the previous three years, and vice versa. Specifically, for the $SO_2$ and CO data, and only data from 2019 were used to calculate the anomalies due to the lack of data for 2017 and 2018.

The MK test was then conducted on the anomalies of six pollutants from January 1 to March 31, 2020 to show the trends. Additionally, to reduce the interference of small fluctuations on the results, an average of the anomalies was taken every three days prior to the MK test.

### Time series analysis for the ground-based data

Similar to the satellite and reanalysis data, first the anomalies of the ground-based AQI data were calculated using the following formula:

$$abAQI_j = AQI_{j,2020} - \sum_{i=2017}^{2019} AQI_{j,i}/3 \quad . \tag{2}$$

Specially, for the AQI data in Tehran, Iran, data from 2017 were lacking, and only data for 2018 and 2019 were used as the baseline. For the $PM_{2.5}$, $NO_2$, and $O_3$ AQIs in Richards Bay, South Africa, data for 2017 and 2018 were lacking, and only data from 2019 were used as the baseline.

For the ground station data, two junctures were researched: time of the first confirmed case ($t_{fc}$), time of lockdown ($t_{lk}$), and one juncture was considered: the time of reopen ($t_{op}$). Two steps were then used to conduct the analysis.

Step one, two quantitative indicators were designed to describe the changes in air quality after the beginning of COVID-19 (time of first case confirmation in the country) and the lockdowns.

$$diff_{1,j} = \sum_{t=t_{fc}}^{t_{lk}-1} abAQI_{j,t}/(t_{lk} - t_{fc}) - \sum_{t=t_0}^{t_{fc}-1} abAQI_{j,t}/(t_{fc} - t_0) \ , \tag{3}$$

$$diff_{2,j} = \sum_{t=t_{lk}}^{t_{op}-1} abAQI_{j,t}/(t_{op} - t_{lk}) - \sum_{t=t_{fc}}^{t_{lk}-1} abAQI_{j,t}/(t_{lk} - t_{fc}) \ , \tag{4}$$

where $j$ represents the types of air pollutants; $diff_1$ and $diff_2$ stand for the changes in the AQI after the first confirmed case and during lockdown, respectively; $t_0$ represents the first day of the total research period, i.e., January 1, 2020; $t_{fc}$, $t_{lk}$, and $t_{op}$ represent the time for first confirmed case in the country, lockdown, and reopen. Then, using the average AQI value during period 1 (from $t_0$ to $t_{fc}$) and period 2 (from $t_{fc}$ to $t_{lk}$) in 2020 as a baseline, the percent of change was calculated:

$$per_{1,j} = \frac{diff_{1,j}}{\sum_{t=t_0}^{t_{fc}-1} AQI_{j,t}/(t_{fc} - t_0)} \times 100\% \ , \tag{5}$$

$$per_{2,j} = \frac{diff_{2,j}}{\sum_{t=t_{fc}}^{t_{lk}-1} AQI_{j,t}/(t_{lk} - t_{fc})} \times 100\% \quad . \tag{6}$$

In step two, a max-mean-value method was used to detect the point where the tendency of time series began to change. To avoid the impact of some extreme values and concentrate on the overall trend, a 15-day moving average for the abnormal AQI time series (*sAQI*) was used. Then,

every time point in the smoothed time series was searched, and the one that had the largest difference the times series before and after the time point in the mean values was located. This process can be expressed as:

$$t_j^* = \arg\max_{t_j^*} \left| \sum_{t=t_0}^{t_j^*-1} sAQI_{j,t} / (t_j^* - t_0) - \sum_{t=t_j^*}^{t_{op}} sAQI_{j,t} / (t_{op} - t_j^* + 1) \right| \quad , \tag{7}$$

where $j$ represents the types of air pollutants; $sAQI$ represents the smoothed abnormal AQI time series after a 15-day moving average; $t^*$ stands for the detected time point and is referred to as the 'change point' in the main text; $t_0$ represents the first day of the total research period, i.e., January 1, 2020; and $t_{op}$ represents the time of reopening (lockdown end). The Pearson correlation coefficients between the change point, FCC, and lockdown times were then calculated.

**Transportation change analysis**

The change in accessible mobility during the entire study period (February 15 to April 24, 2020) was divided into two parts: change after the first case confirmation and change after the lockdown began. The contribution of each part to the total decline in mobility was calculated using the following formula:

$$dTrans_1 = diff_{1,Trans} / (diff_{1,Trans} + diff_{2,Trans}) \ , \tag{8}$$

$$dTrans_2 = diff_{2,Trans} / (diff_{1,Trans} + diff_{2,Trans}) \ , \tag{9}$$

where $dTans_1$ and $dTrans_2$ represent the contribution of the first case confirmation and the lockdown to the total decline in mobility, respectively. In addition,

$$diff_{1,\mathrm{Trans}} = \sum_{t=t_{fc}}^{t_{lk}\text{-}1} Trans_t / (\mathrm{t}_{lk}\text{-}\mathrm{t}_{fc}) - \sum_{t=t_0}^{t_{fc}-1} Trans_t / (t_{fc} - t_0) \, , \tag{10}$$

$$diff_{2,\mathrm{Trans}} = \sum_{t=t_{lk}}^{t_{op}-1} Trans_t / (t_{op} - t_{lk}) - \sum_{t=t_{fc}}^{t_{lk}\text{-}1} Trans_{j,t} / (\mathrm{t}_{lk}\text{-}\mathrm{t}_{fc}) \quad , \tag{11}$$

where $Trans_t$ represents the mobility at day $t$.

**Meteorological change analysis**

The analysis of meteorological condition changes during this time period was similar to that of the ground-based AQI data, which included two primary steps. First, the anomalies of 2020 were calculated using the average value of 2017–2019 as the baseline. Then the variations in the daily anomalies in 2020 were divided into two parts: change after the first case confirmation and change after the lockdown started, which are calculated in the same way as the AQI change and transportation change. The composite wind speed (WS) was calculated from the zonal wind (UWS) and meridional wind (VWS) using the following formula:

$$WS = \sqrt{UWS^2 + VWS^2}\,. \tag{12}$$

**The Mann-Kendall (MK) test**

As a non-parametric statistical test method, MK does not require samples to follow a certain distribution and not be disturbed by a few outliers[54]. It is often applied to trend analyses and mutation detections in time series. Assuming that $X_1, X_2..., X_n$ is a set of time-series data, the test statistic, S, is defined by the following equations:

$$S = \sum_{i=2}^{n} \sum_{j=1}^{i-1} sign(X_i - X_j)\,, \tag{13}$$

$$sign(X_i - X_j) = \begin{cases} 1, (X_i - X_j) > 0 \\ 0, (X_i - X_j) = 0 \\ -1, (X_i - X_j) < 0 \end{cases}, \tag{14}$$

$$vars(S) = n(n-1)(2n+5)/18\,, \tag{15}$$

where S is normally distributed with a mean of 0; and vars(S) is the variance of S.

Then the Z statistic is calculated to indicate variation trends of the time series data if n was greater than 10:

$$Z = \begin{cases} \dfrac{S-1}{\sqrt{var(S)}}, S > 0 \\ 0, S = 0 \\ \dfrac{S+1}{\sqrt{var(S)}}, S < 0 \end{cases}. \tag{16}$$

The variation trend of a time series manifests as an increasing tendency when Z is positive, while a negative Z indicates a decreasing tendency. Additionally, the variation trend is significant (95% significance level) when the absolute value of Z exceeds 1.64 and is extremely significant (95% significance level) when the absolute value of Z exceeds 2.32.

## Acknowledgments

We thank all of the individuals and organizations who collected air quality data and other relevant data during the COVID-19 outbreak around the world. We gratefully acknowledge the support from the Strategic Priority Research Program of the Chinese Academy of Sciences (No. XDA19090104) and the National Natural Science Foundation of China (Nos. 41922008).

## Author contributions

L.Z. and Qiangqiagn Yuan conceived the study. Qiangqiang Yuan, Qianqian Yang, B.W., and Y.W. developed the methods, collected the data, performed analyses, and co-wrote the manuscript, and they contributed equally to this work. T.L., C.J., J.W., S.L., and M.L. contributed to the data analysis and interpretation of the results. L.Z., H.S., and Qiangqiang Yuan reviewed and edited the manuscript.

## Declaration of interests

The authors declare no competing interests.

## References

1. Klepeis, N.E., Nelson, W.C., Ott, W.R., Robinson, J.P., Tsang, A.M., Switzer, P., Behar, J. V, Hern, S.C., And Engelmann, W.H. (2001). The National Human Activity Pattern Survey (NHAPS): a resource for assessing exposure to environmental pollutants. J. Expo. Sci. Environ. Epidemiol. 11, 231–252.

2. Ezzati, M., Lopez, A. D., Rodgers, A. A., Murray, C. J. (2004). Comparative quantification of health risks: global and regional burden of disease attributable to selected major risk factors. World Health Organization.

3. Brunekreef, B., and Holgate, S.T. (2002). Air pollution and health. Lancet 360, 1233–1242.

4. Cohen, A.J., Brauer, M., Burnett, R., Anderson, H.R., Frostad, J., Estep, K., Balakrishnan, K., Brunekreef, B., Dandona, L., Dandona, R., et al. (2017). Estimates and 25-year trends of the global burden of disease attributable to ambient air pollution: an analysis of data from the Global Burden of Diseases Study 2015. Lancet 389, 1907–1918.

5. Ambient air pollution, World Health Organization. https://www.who.int/airpollution/ambient/health-impacts/en/ [accessed 9 October 2020]

6. Akimoto, H. (2003). Global Air Quality and Pollution. Science 302(5651), 1716–1719.

7. Team, T.N.C.P.E.R.E. The Epidemiological Characteristics of an Outbreak of 2019 Novel Coronavirus Diseases (COVID-19) — China, 2020. China CDC Wkly. 2, 113–122.

8. Zhu, N., Zhang, D., Wang, W., Li, X., Yang, B., Song, J., Zhao, X., Huang, B., Shi, W., Lu, R., et al. (2020). A Novel Coronavirus from Patients with Pneumonia in China, 2019. N. Engl. J. Med. 382, 727–733.

9. Guan, W., Ni, Z., Hu, Y., Liang, W., Ou, C., He, J., Liu, L., Shan, H., Lei, C., Hui, D.S.C., et al. (2020). Clinical Characteristics of Coronavirus Disease 2019 in China. N. Engl. J. Med. 382, 1708–1720.

10. Remuzzi, A., and Remuzzi, G. (2020). COVID-19 and Italy: what next? Lancet 395, 1225–1228.

11. Mizumoto, K., Kagaya, K., Zarebski, A., and Chowell, G. (2020). Estimating the asymptomatic proportion of coronavirus disease 2019 (COVID-19) cases on board the Diamond Princess cruise ship, Yokohama, Japan, 2020. Eurosurveillance 25.

12. COVID, CDC, and Response Team. (2020). Severe outcomes among patients with coronavirus disease 2019 (COVID-19)—United States, February 12–March 16, 2020. MMWR Morb Mortal Wkly Rep, 69(12), 343-346.

13. Sohrabi, C., Alsafi, Z., O'Neill, N., Khan, M., Kerwan, A., Al-Jabir, A., Iosifidis, C., and Agha, R. (2020). World Health Organization declares global emergency: A review of the 2019 novel coronavirus (COVID-19). Int. J. Surg. 76, 71–76.

14. Anderson, R.M., Heesterbeek, H., Klinkenberg, D., and Hollingsworth, T.D. (2020). How will country-based mitigation measures influence the course of the COVID-19 epidemic? Lancet 395, 931–934.

15. World Health Organization. (2020). Assessment of risk factors for coronavirus disease 2019 (COVID-19) in health workers: protocol for a case-control study, 26 May 2020 (No. WHO/2019-nCoV/HCW_RF_CaseControlProtocol/2020.1). World Health Organization.

16. Wu, Z., and McGoogan, J.M. (2020). Characteristics of and Important Lessons from the Coronavirus Disease 2019 (COVID-19) Outbreak in China: Summary of a Report of 72 314 Cases From the Chinese Center for Disease Control and Prevention. JAMA 323, 1239–1242.

17. World Health Organization, Coronavirus disease (COVID-2019) situation reports; https://www.who.int/emergencies/diseases/novel-coronavirus-2019/situation-reports/ [accessed 9 October 2020]

18. Tian, H., Liu, Y., Li, Y., Wu, C.-H., Chen, B., Kraemer, M.U.G., Li, B., Cai, J., Xu, B., Yang, Q., et al. (2020). An investigation of transmission control measures during the first 50 days of the COVID-19 epidemic in China. Science. 368, 638 – 642.

19. Chinazzi, M., Davis, J.T., Ajelli, M., Gioannini, C., Litvinova, M., Merler, S., Pastore y Piontti, A., Mu, K., Rossi, L., Sun, K., et al. (2020). The effect of travel restrictions on the spread of the 2019 novel coronavirus (COVID-19) outbreak. Science. 368, 395– 400.

20. Saraswat, R., and Saraswat, D.A. (2020). Research opportunities in pandemic lockdown. Science. 368, 594 – 595.

21. Rosenbloom, D., and Markard, J. (2020). A COVID-19 recovery for climate. Science. 368, 447 – 447.

22. He, G., Pan, Y., and Tanaka, T. (2020). The short-term impacts of COVID-19 lockdown on urban air pollution in China. Nat. Sustain. https://doi.org/10.1038/s41893-020-0581-y

23. Mahato, S., Pal, S., and Ghosh, K.G. (2020). Effect of lockdown amid COVID-19 pandemic on air quality of the megacity Delhi, India. Sci. Total Environ. 730, 139086.

24. Wang, Q., and Su, M. (2020). A preliminary assessment of the impact of COVID-19 on environment – A case study of China. Sci. Total Environ. 728, 138915.

25. Sharma, S., Zhang, M., Anshika, Gao, J., Zhang, H., and Kota, S.H. (2020). Effect of restricted emissions during COVID-19 on air quality in India. Sci. Total Environ. 728, 138878.

26. Huang, X., Ding, A., Gao, J., Zheng, B., Zhou, D., Qi, X., Tang, R., Wang, J., Ren, C., Nie, W. (2020). Enhanced secondary pollution offset reduction of primary emissions during COVID-19 lockdown in China. National Science Review.

27. Shi, X., Brasseur., G.P. (2020). The response in air quality to the reduction of Chinese economic activities during the COVID-19 outbreak, Geophys. Res. Lett., 47 (11), e2020GL088070.

28. Bauwens, M., Compernolle, S., Stavrakou, T., Müller, J.-F., van Gent, J., Eskes, H., Levelt, P.F., van der A, R., Veefkind, J.P., Vlietinck, J., et al. (2020). Impact of Coronavirus Outbreak on NO2 Pollution Assessed Using TROPOMI and OMI Observations. Geophys. Res. Lett. 47, e2020GL087978.

29. Chen, H., Huo, J., Fu, Q., Duan, Y., Xiao, H., Chen, J. (2020). Impact of quarantine measures on chemical compositions of PM2.5 during the COVID-19 epidemic in Shanghai, China. Sci. Total Environ., 743, 140758.

30. Rodríguez-Urrego, D., Rodríguez-Urrego, L. (2020). Air quality during the COVID-19: PM2.5 analysis in the 50 most polluted capital cities in the world. Environ. Pollut., 115042.

31. Chu, B., Zhang, S., Liu, J., Ma, Q., He, H. (2020). Significant concurrent decrease in PM2.5 and NO2 concentrations in China during COVID-19 epidemic. Journal of Environ. Sci., 99, 346-353.

32. Venter, Z. S., Aunan, K., Chowdhury, S., Lelieveld, J. (2020). COVID-19 lockdowns cause global air pollution declines. P. Natl. Acad. Sci. USA., 117(32), 18984-18990.

33. Diffenbaugh, N. S., Field, C. B., Appel, E. A., Azevedo, I. L., Baldocchi, D. D., Burke, M., Burney, J. A., Ciais, P., Davis, S. J., Fiore, A. M. et al. (2020). The COVID-19 lockdowns: a window into the Earth System, Nature Reviews Earth Environment, 1, 470–481.

34. Zhang, Z., Arshad, A., Zhang, C., Hussain, S., Li, W. (2020). Unprecedented temporary reduction in global air pollution associated with COVID-19 forced confinement: A continental and city scale analysis. Remote Sens., 12(15), 2420.

35. Guan, Q., Yang, Y., Luo, H., Zhao, R., Pan, N., Lin, J., Yang, L. (2019). Transport pathways of PM10 during the spring in northwest China and its characteristics of potential dust sources. J. Cleaner Prod. 237(10), 117746.

36. Hashem, T. M., Zirlewagen, M., & Braun, A. M. (1997). Simultaneous photochemical generation of ozone in the gas phase and photolysis of aqueous reaction systems using one VUV light source. Water Science and Technology, 35(4), 41-48.

37. Saglietto, A., D'Ascenzo, F., Zoccai, G.B., and De Ferrari, G.M. (2020). COVID-19 in Europe: the Italian lesson. Lancet 395, 1110–1111.

38. Kupferschmidt, K., and Cohen, J. (2020). Can China's COVID-19 strategy work elsewhere? Science. 367, 1061–1062.

39. Le, T., Wang, Y., Liu, L., Yang, J., Yung, Y. L., Li, G., Seinfeld, J. H. (2020). Unexpected air pollution with marked emission reductions during the COVID-19 outbreak in China. Science, 369(6504), 702-706.

40. Kota, S.H., Guo, H., Myllyvirta, L., Hu, J., Sahu, S.K., Garaga, R., Ying, Q., Gao, A., Dahiya, S., Wang, Y., et al. (2018). Year-long simulation of gaseous and particulate air pollutants in India. Atmos. Environ. 180, 244–255.

41. Arif, M., Kumar, R., Kumar, R., Eric, Z., and Gourav, P. (2018). Ambient black carbon, PM2.5 and PM10 at Patna: Influence of anthropogenic emissions and brick kilns. Sci. Total Environ. 624, 1387–1400.

42. Ripperton, L. A., Kornreich, L., Worth, J. J. (1970). Nitrogen dioxide and nitric oxide in non-urban air. Journal of the Air Pollution Control Association, 20(9), 589-592.

43. Han, S., Bian, H., Feng, Y., Liu, A., Li, X., Zeng, F., Zhang, X. (2011). Analysis of the Relationship between O3, NO and NO2 in Tianjin, China. Aerosol and Air Quality Research, 11(2), 128-139.

44. Wang, T., Cheung, V.T.F., Anson, M., Li, Y.S. (2001). Ozone and related gaseous pollutants in the boundary layer of eastern China: Overview of the recent measurements at a rural site. Geophys. Res. Lett. 28, 2373–2376.

45. Hashim, B. M., Al-Naseri, S. K., Al-Maliki, A., Al-Ansari, N. (2020). Impact of COVID-19 lockdown on NO2, O3, PM2.5 and PM10 concentrations and assessing air quality changes in Baghdad, Iraq. Sci. Total Environ., 141978.

46. Melkonyan, A., and Kuttler, W. (2012). Long-term analysis of NO, NO2 and O3 concentrations in North Rhine-Westphalia, Germany. Atmos. Environ. 60, 316–326.

47. Li, T., Shen, H., Yuan, Q., Zhang, X., and Zhang, L. (2017). Estimating Ground-Level PM2.5 by Fusing Satellite and Station Observations: A Geo-Intelligent Deep Learning Approach. Geophys. Res. Lett. 44, 11,911-985,993.

48. Wang, Z., Li, Y., Chen, T., Zhang, D., Sun, F., Wei, Q., Dong, X., Sun, R., Huan, N., and Pan, L. (2015). Ground-level ozone in urban Beijing over a 1-year period: Temporal variations and relationship to atmospheric oxidation. Atmos. Res. 164–165, 110–117.

49. Wotawa, G., and Trainer, M. (2000). The Influence of Canadian Forest Fires on Pollutant Concentrations in the United States. Science. 288, 324–328.

50. Berman, J. D., Ebisu, K. (2020). Changes in U.S. air pollution during the COVID-19 pandemic. Sci. Total Environ. 739(15), 139864.

51. Liu, F., Page, A., Strode, S. A., Yoshida, Y., Choi, S., Zheng, B., Lamsal, L. N., Li, C., Krotkov, N. A., Eskes, H. (2020). Abrupt decline in tropospheric nitrogen dioxide over China after the outbreak of COVID-19. Sci. Adv. 6(28), eabc2992.

52. Chen, K., Wang, M., Huang, C., Kinney, P. L., Anastas, P. T. (2020). Air pollution reduction and mortality benefit during the COVID-19 outbreak in China. Lancet Planet. Health 4(6), e210-e212.

53. Gillingham, K. T., Knittel, C. R., Li, J., Ovaere, M., & Reguant, M. (2020). The Short-run and Long-run Effects of Covid-19 on Energy and the Environment. Joule, 4(7), 1337-1341.

54. Yue, S., Pilon, P., and Cavadias, G. (2002). Power of the Mann–Kendall and Spearman's rho tests for detecting monotonic trends in hydrological series. J. Hydrol. 259, 254–271.

# Supplemental files for: Global air quality change during COVID-19: a synthetic result of human activities and meteorology

**Qianqian Yang[1,*], Bin Wang[1,*], Yuan Wang[1,*], Qiangqiang Yuan[1,*], Caiyi Jin[1], Jiwen Wang[1], Shuwen Li[1], Muyu Li[1], Tongwen Li[2,†], Song Liu[3], Huanfeng Shen[2], Liangpei Zhang[4]**

[1] School of Geodesy and Geomatics, Wuhan University, Wuhan, China.

[2] School of Resource and Environmental Sciences, Wuhan University, Wuhan, China.

[3] Deutsches Zentrum für Luft- und Raumfahrt (DLR), Institut für Methodik der Fernerkundung (IMF), Oberpfaffenhofen, Germany

[4] State Key Laboratory of Information Engineering in Surveying, Mapping and Remote Sensing, Wuhan University, Wuhan, China.

Corresponding author: Qiangqiang Yuan (qqyuan@sgg.whu.edu.cn); Huanfeng Shen (shenhf@whu.edu.cn); Liangpei Zhang (zlp62@whu.edu.cn).

[*]These authors contributed equally: Qianqian Yang, Bin Wang, Yuan Wang, Qiangqiang Yuan.

†Present address: School of Geospatial Engineering and Science, Sun Yat-Sen University, Guangzhou, China

**Contents:**

Supplemental Figures: Figure S1-14

Supplemental Tables: Table S1-4

Supplemental Materials and Method

Supplemental References

# Supplemental Figures

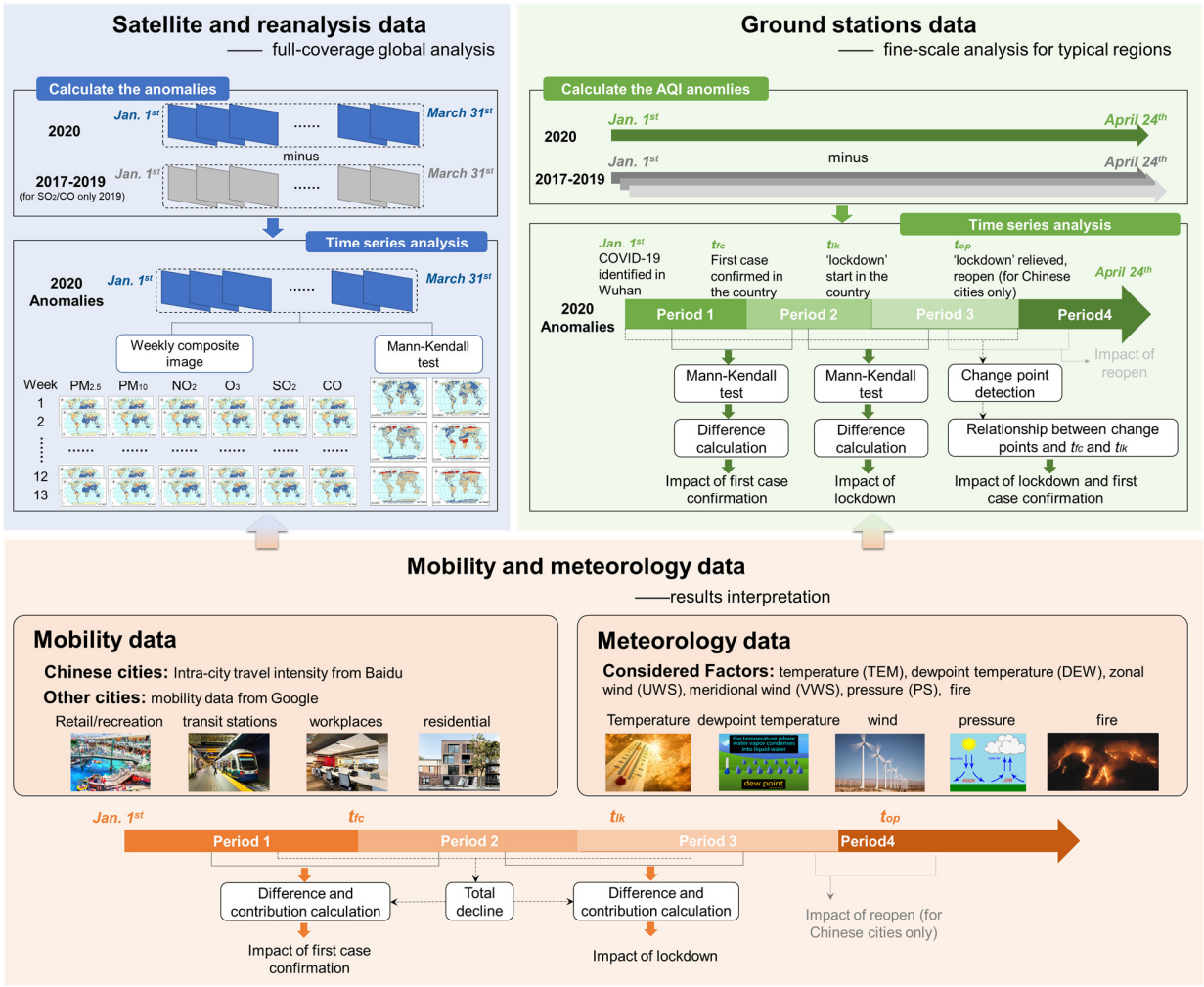


**Figure S1.** Flowchart of the work. Firstly, for a full-coverage investigation of the global air quality change were analyzed using satellite and reanalysis data via MK test. Secondly, for a fine-scale analysis of typical regions, we selected 26 typical cities around the world and analyzed the air quality index (AQI) data of six main atmospheric pollutants from local environmental monitoring stations. Finally, combined with the mobility and meteorology data, we tried to make a better explanation of the conclusions we got.

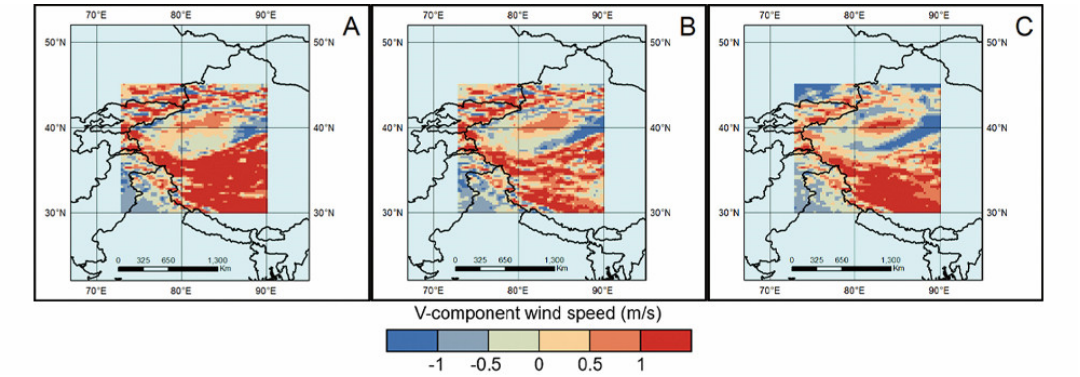


**Figure S2.** The v-component wind speed (VWS) in Qinghai-Tibet Plateau. A-C represent VWS for Jan. 2020 to Mar. 2020, respectively.

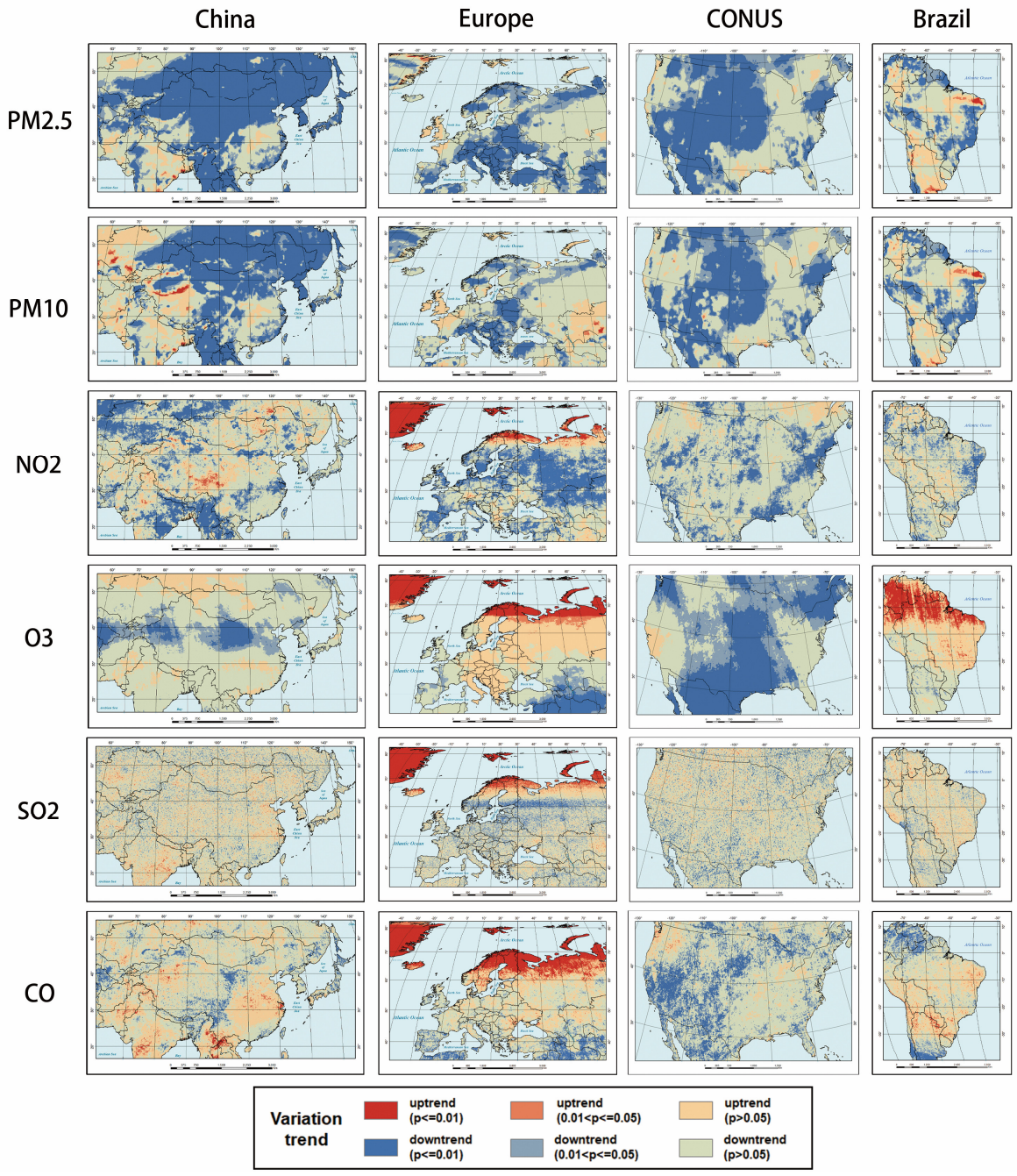


**Figure S3.** Variation trends for six pollutants anomalies in China, Europe, and CONUS. Each column represents a country, and each row represents a pollutant. All trends and significances were calculated by MK test.

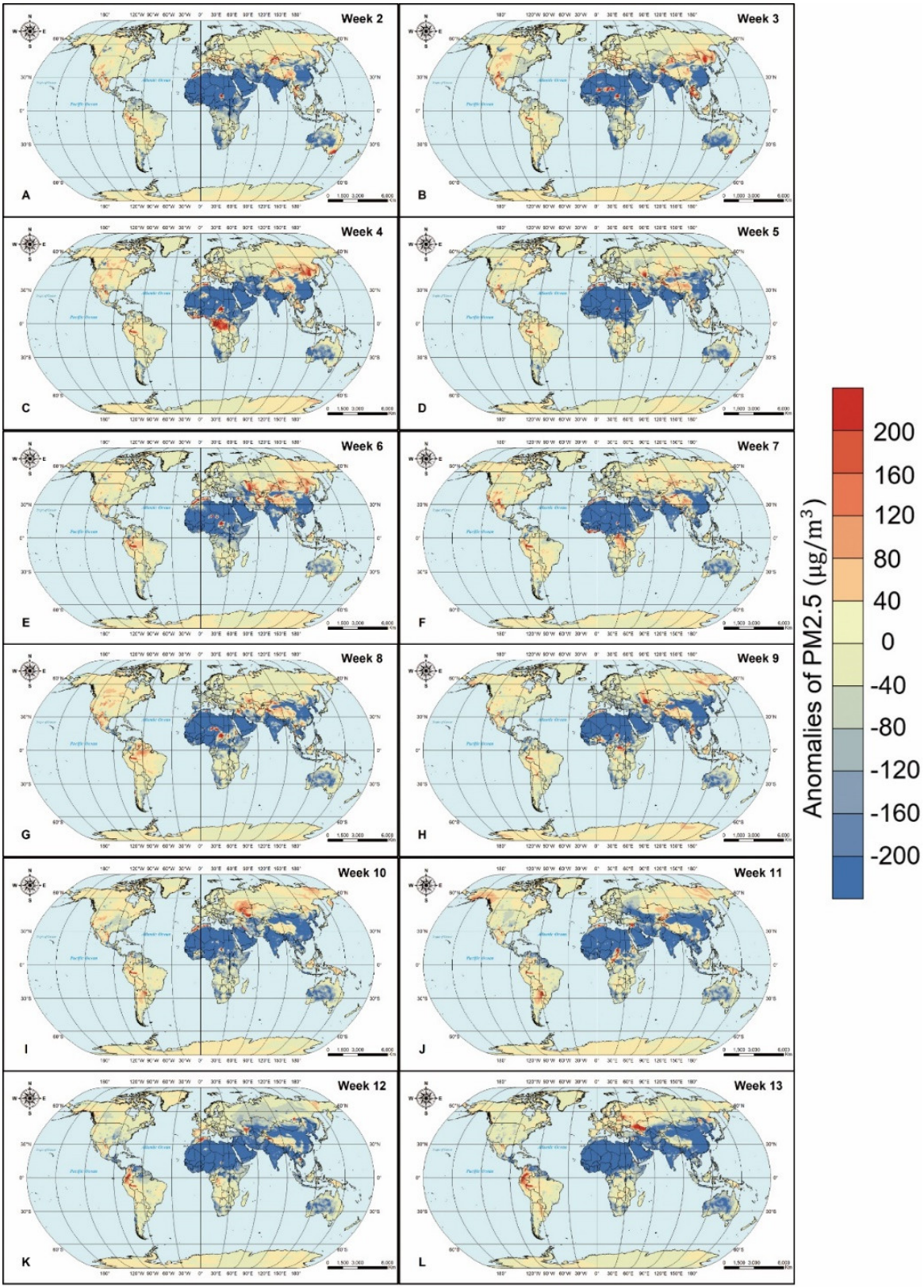


**Figure S4.** Global weekly averaged values of $PM_{2.5}$ anomalies. (A-L) represent the results in different weeks since Jan. 1, 2020.

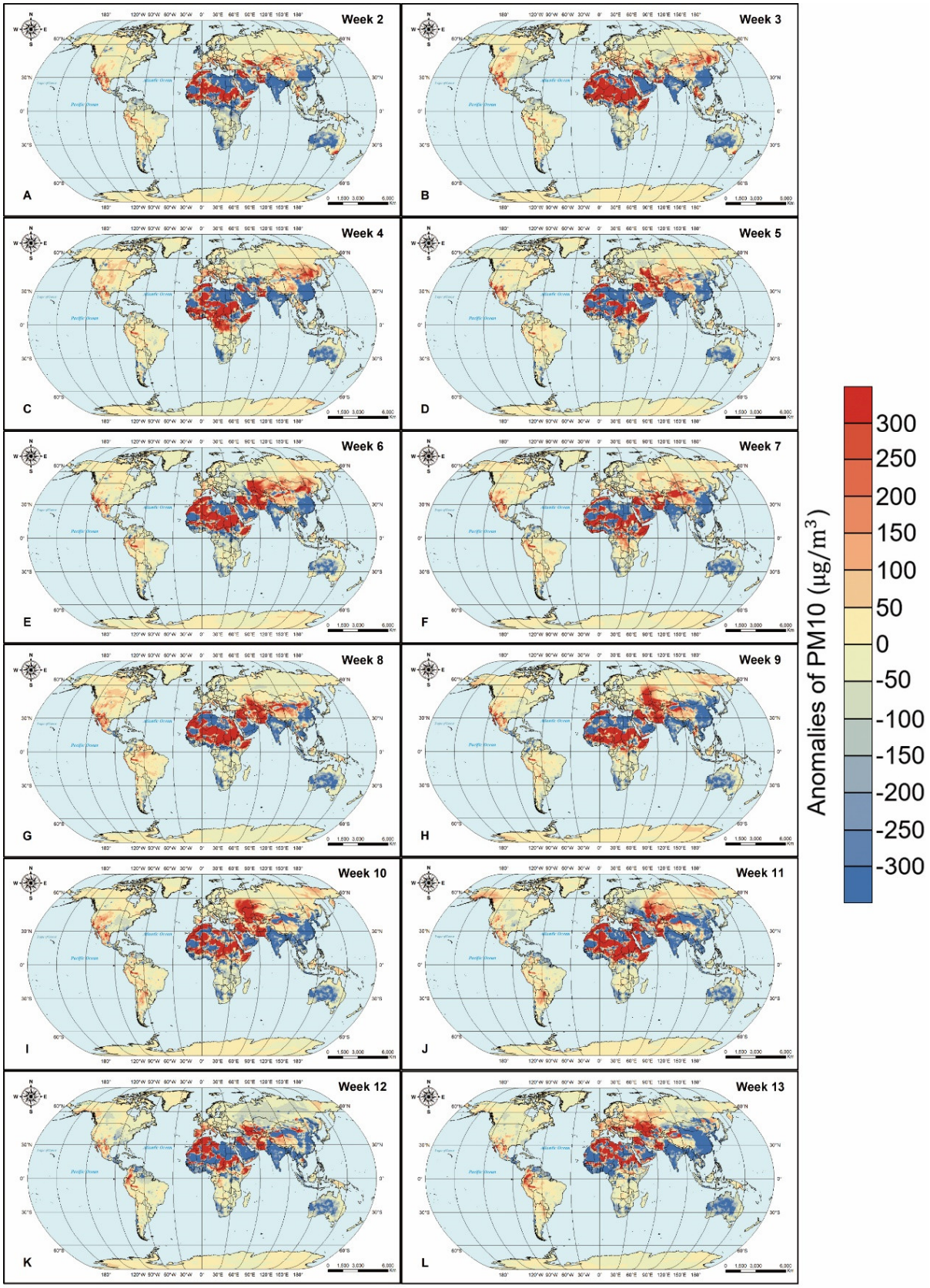


**Figure S5.** Global weekly averaged values of $PM_{10}$ anomalies. (A-L) represent the results in different weeks since Jan. 1, 2020.

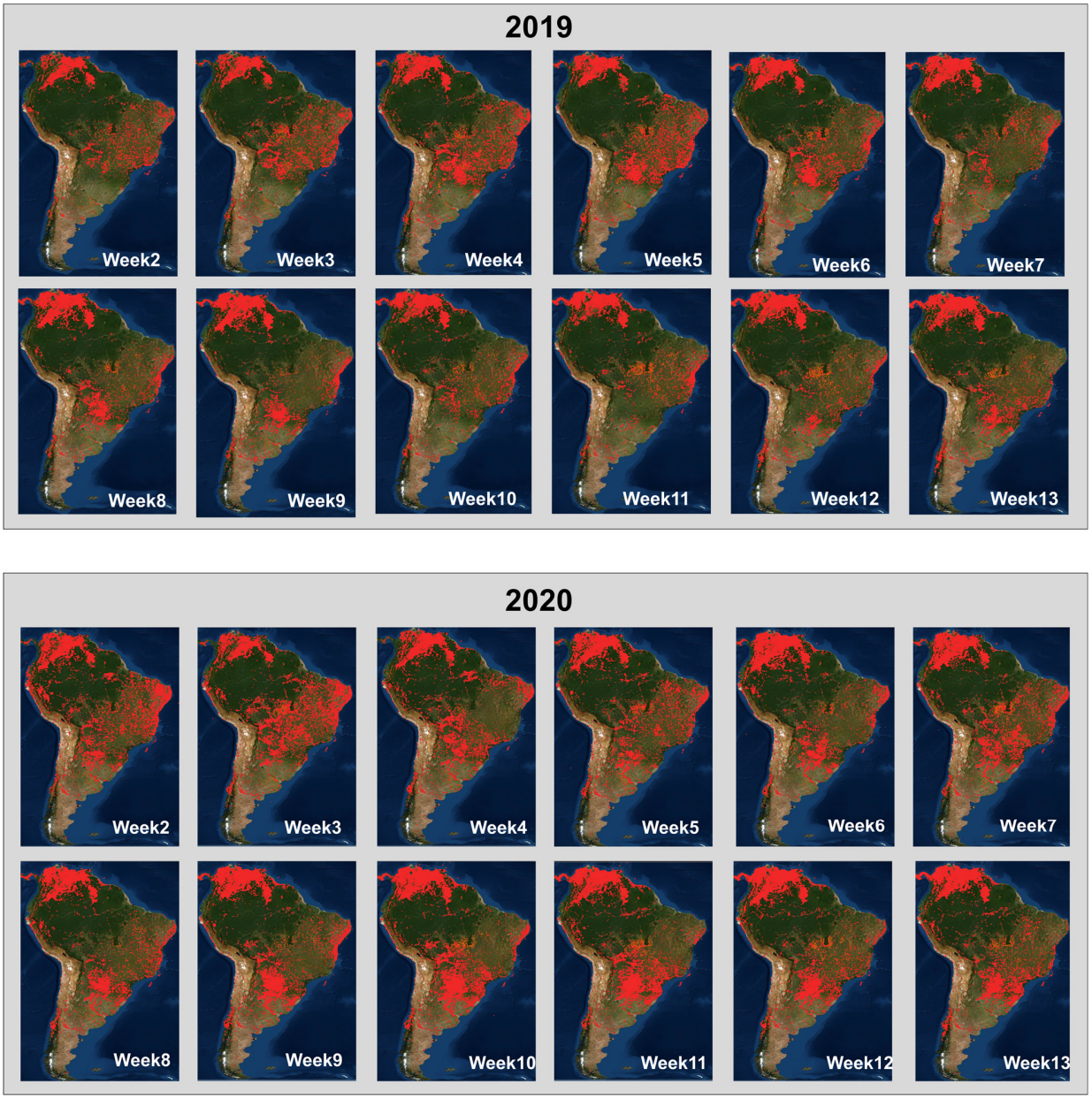


**Figure S6.** Global weekly averaged fire data for 2019 and 2020. The data were provided by Fire Information for Resource Management System (https://firms.modaps.eosdis.nasa.gov/map/#d:2020-10-17..2020-10-18;@0.0,0.0,3z)

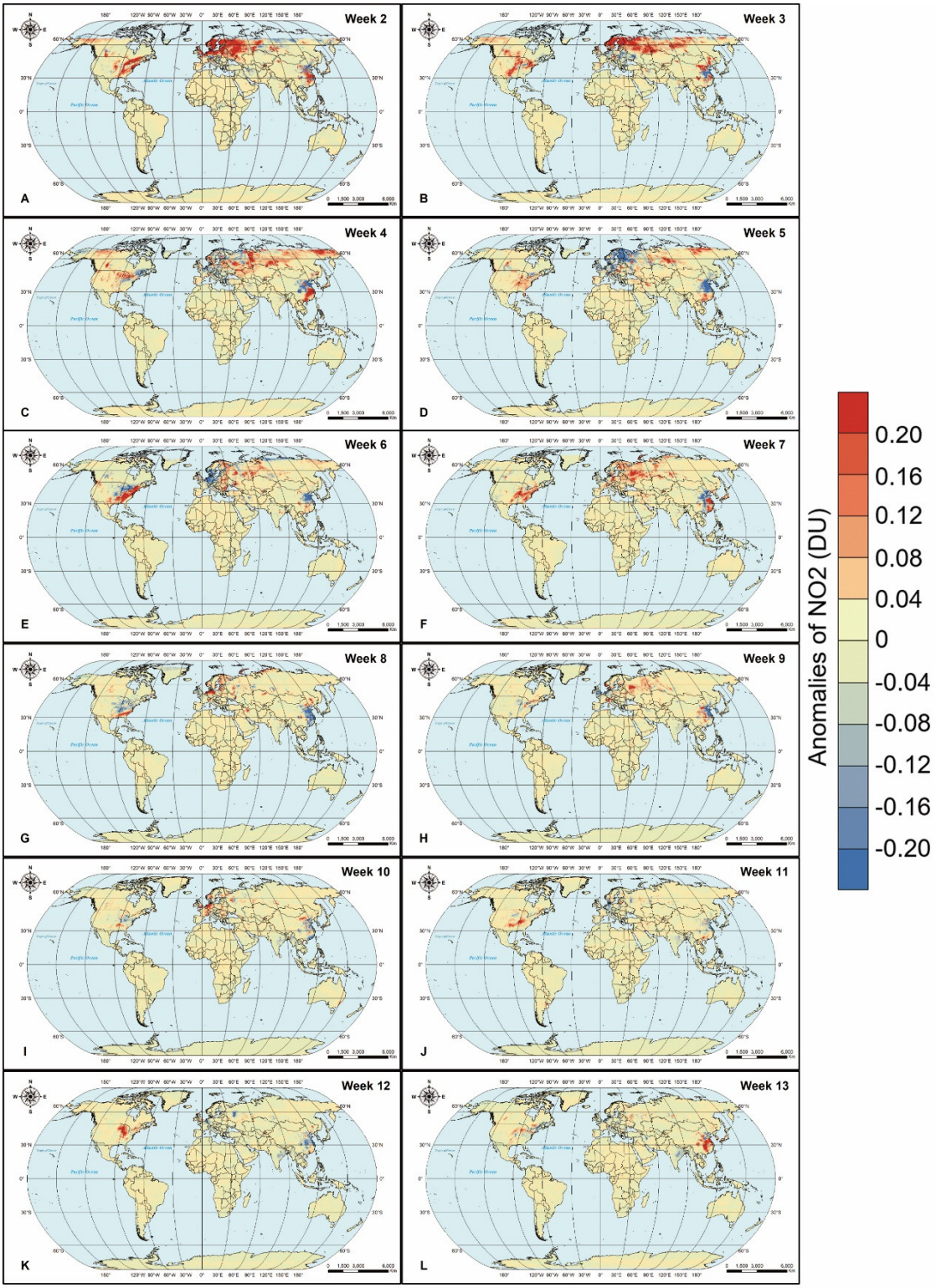


**Figure S7.** Global weekly averaged values of $NO_2$ anomalies. (A-L) represent the results in different weeks since Jan. 1, 2020.

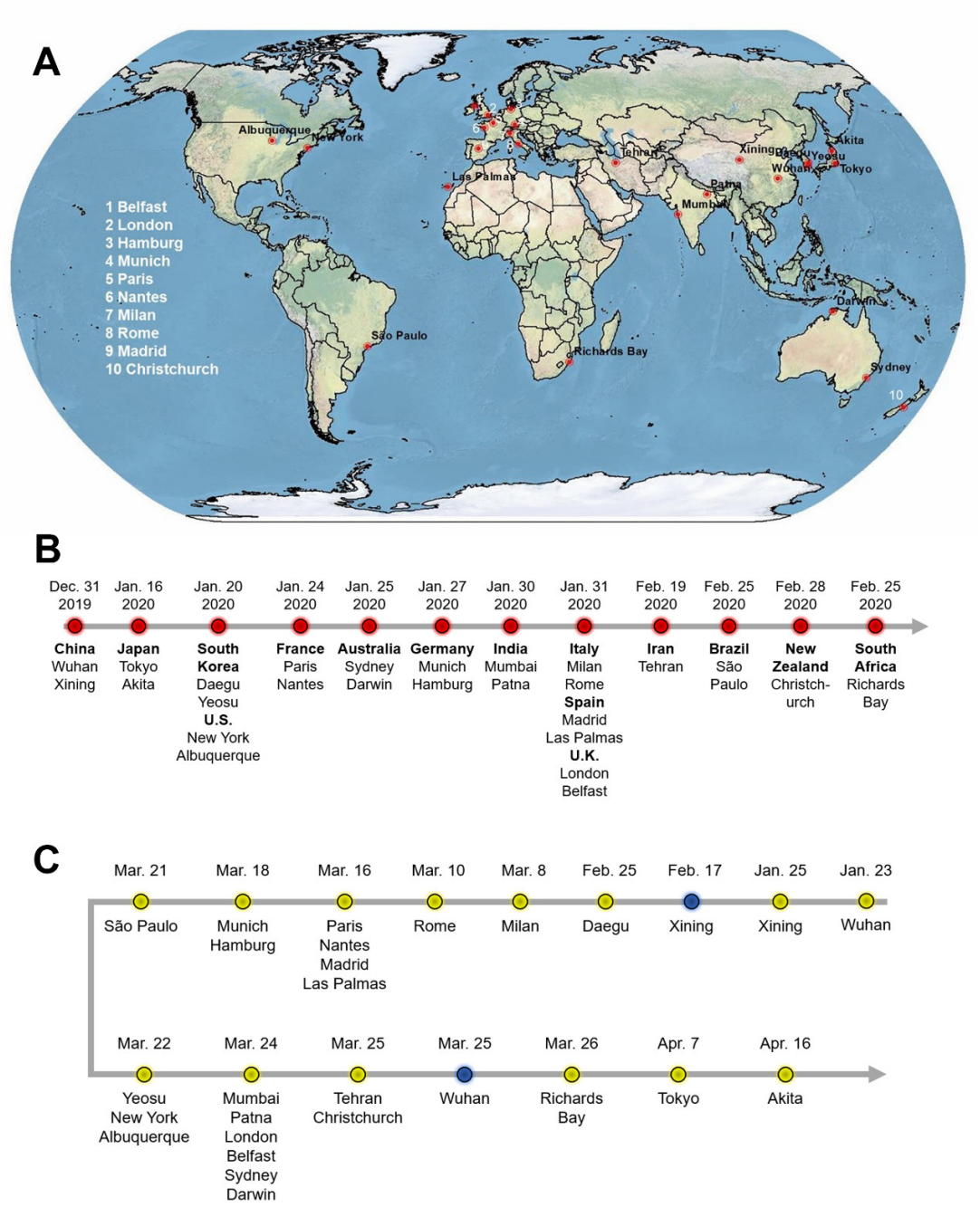


**Figure S8.** Distribution of the selected cities and their FCC time and lockdown time. (A) The spatial distribution of selected 26 cities. Cities in Europe and New Zealand are numbered to avoid congestion and the numbers for cities are on the left side of the map. (B) Times when the first case was confirmed in each city and its country (bold). (C) Times when the government declare a lockdown or other equivalent restrictions of each city. Especially, for two cities in China, we display their resumption time additionally, which were represented by blue point.

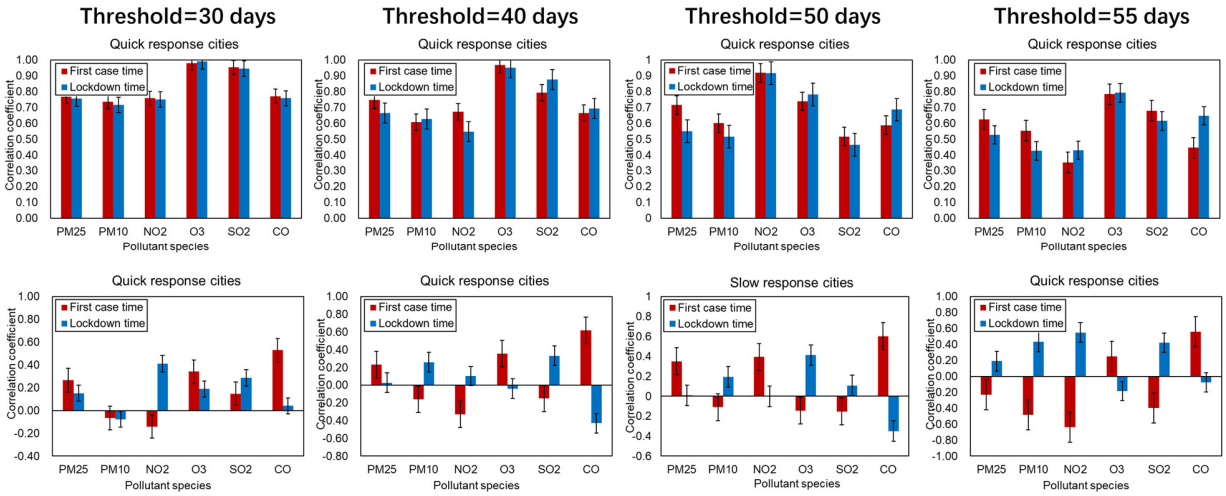


**Figure S9.** The parameter sensitivity test results for determining the number of days to differentiate slow- and quick-response cities. We set the threshold as 30 days, 40 days, 50 days, 55 days respectively to distinguish the quick- and slow-response cities, and then observed the correlation between change point and FCC/lockdown time in two group of cities. Then we found the conclusion can be relatively steady with the thresholds changing. The threshold was not set as 60 days because under this case the number of slow-response cities can be too small to analyze.

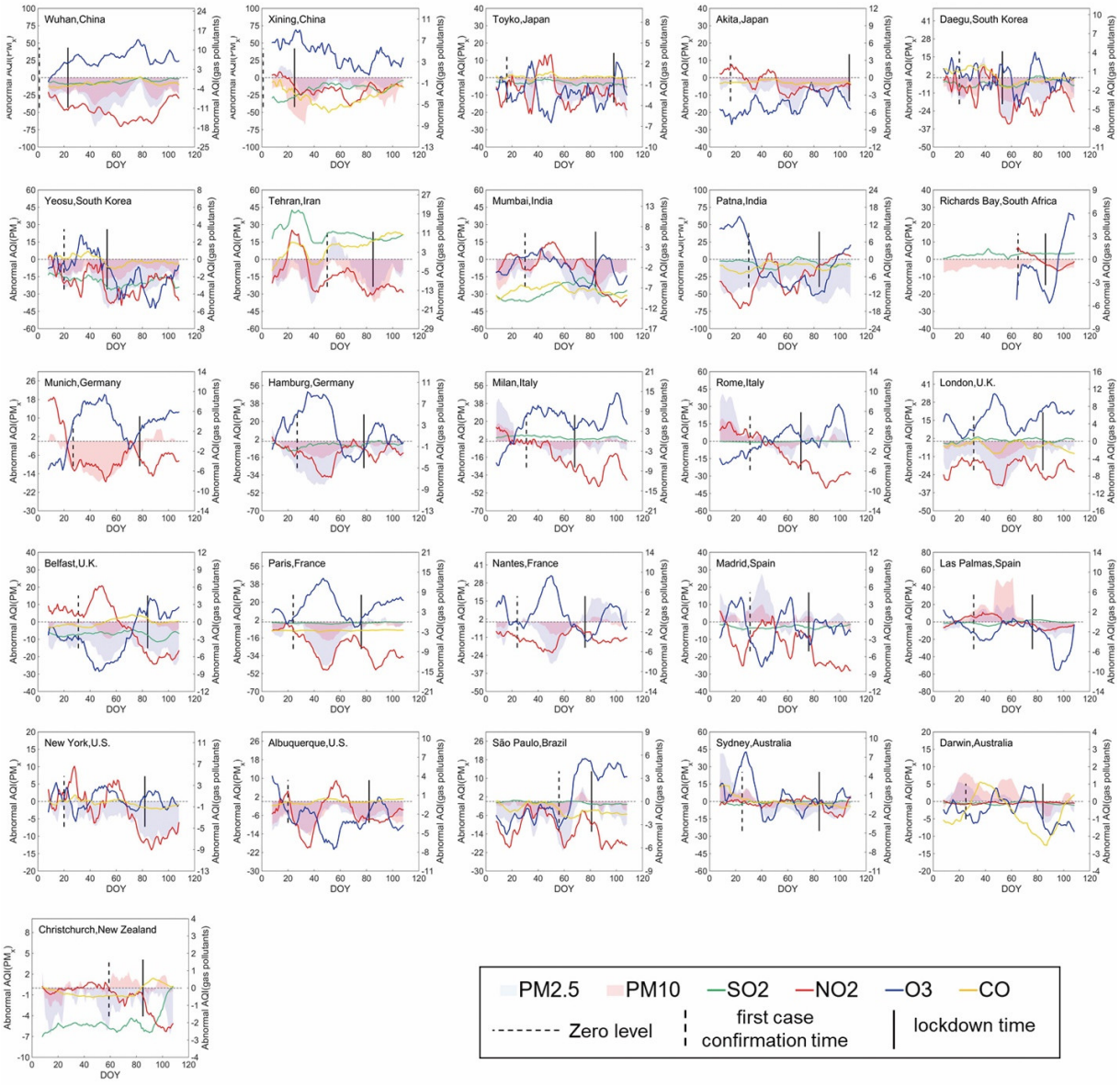


**Figure S10.** 15-day moving average trend of abnormal AQI data of six pollutants in 26 cities. The dashed vertical lines represent the first case confirmation time and the solid vertical lines represent lockdown time. The horizonal dashed lines are the y=0 lines, which indicate no change of AQI.

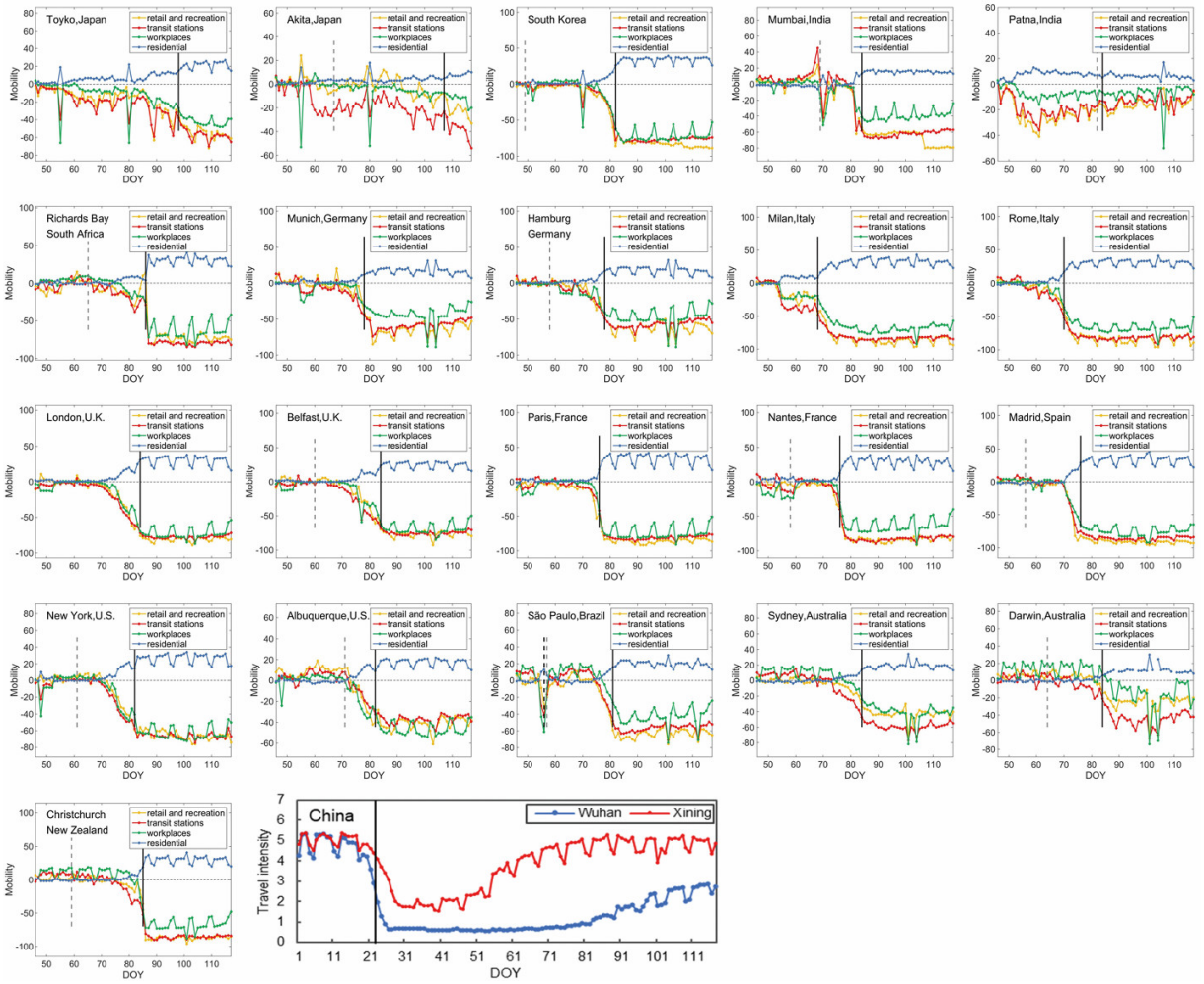


734

735 **Figure S11.** Time series of mobility data in 21 cities and the intra-city travel intensity data for two
736 cities in China. In the first 21 subgraphs, the yellow lines, red lines, green lines, and blue lines
737 represent the mobility variation of retail and recreation, transit stations, workplaces, and residential,
738 respectively. While in the last subgraph, the blue and red lines represent the intra-city travel
739 intensity variations in Wuhan and Xining, respectively. The black and grey dashed vertical lines
740 represent the first case confirmation time of the country and of local region, the solid vertical lines
741 represent lockdown time. If the confirmation time or lockdown time is beyond the period of Feb.
742 15 to Apr. 24 then it was not displayed in the figure.
743

744

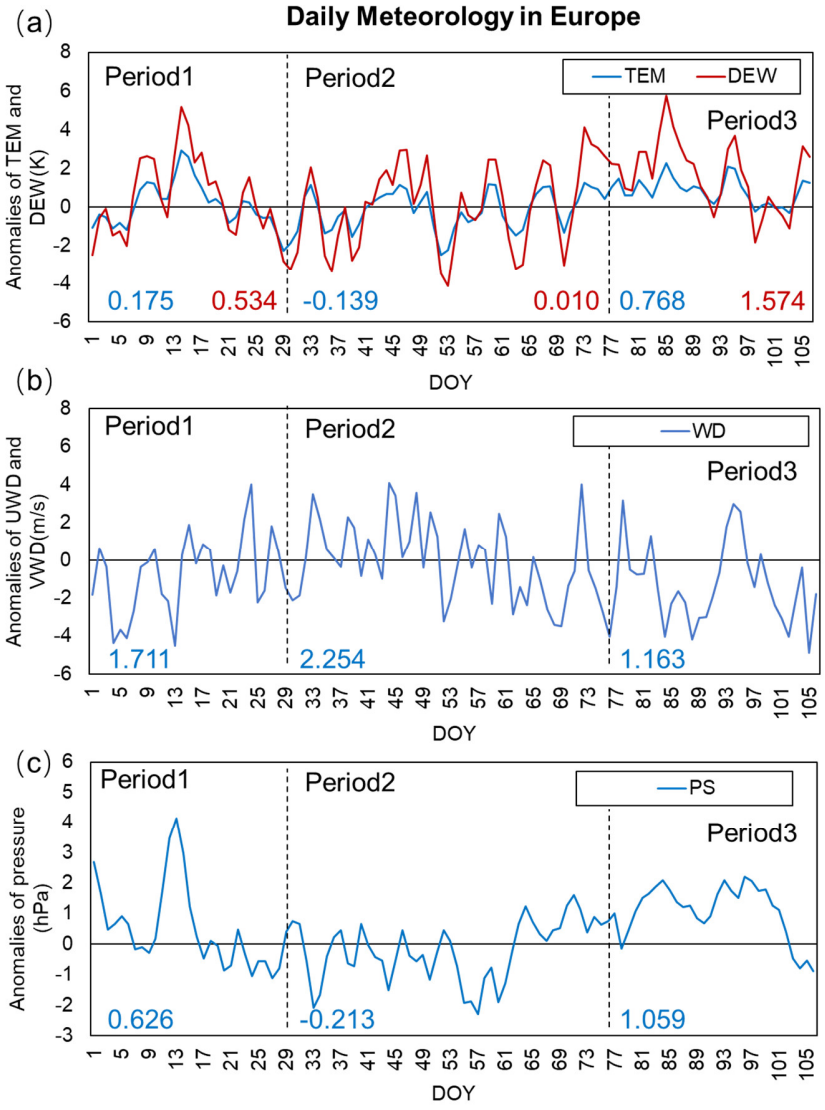


**Figure S12.** The daily variations of meteorological anomalies in 2020 in Europe. The blue and red numbers represent the mean values of the corresponding meteorological parameter in each period. The dashed black lines represent the mean FCC and lockdown time of the Europe cities.

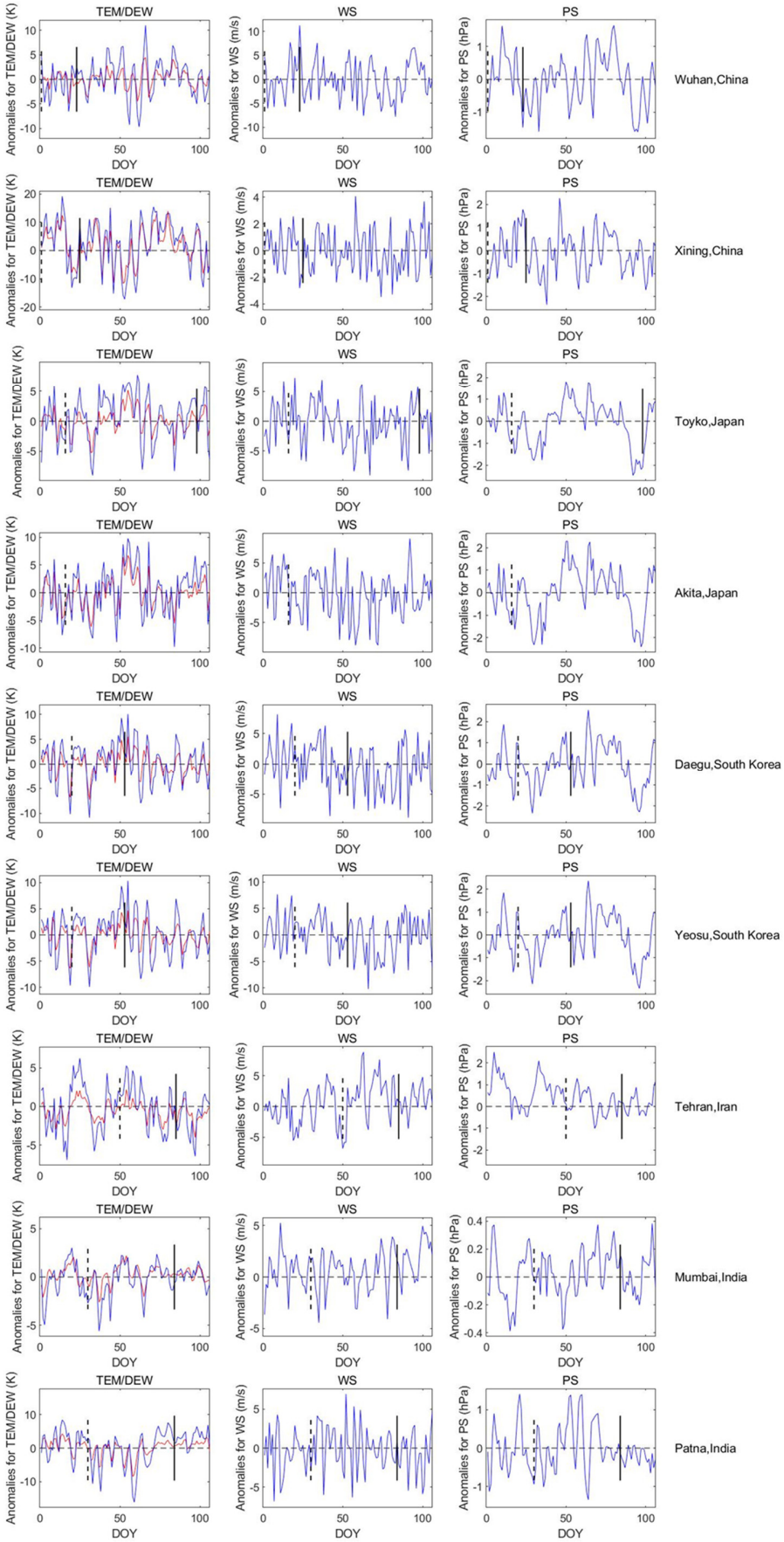


**Figure S13(1).** The daily variations of meteorological anomalies in 2020 in the 26 cities—part 1.

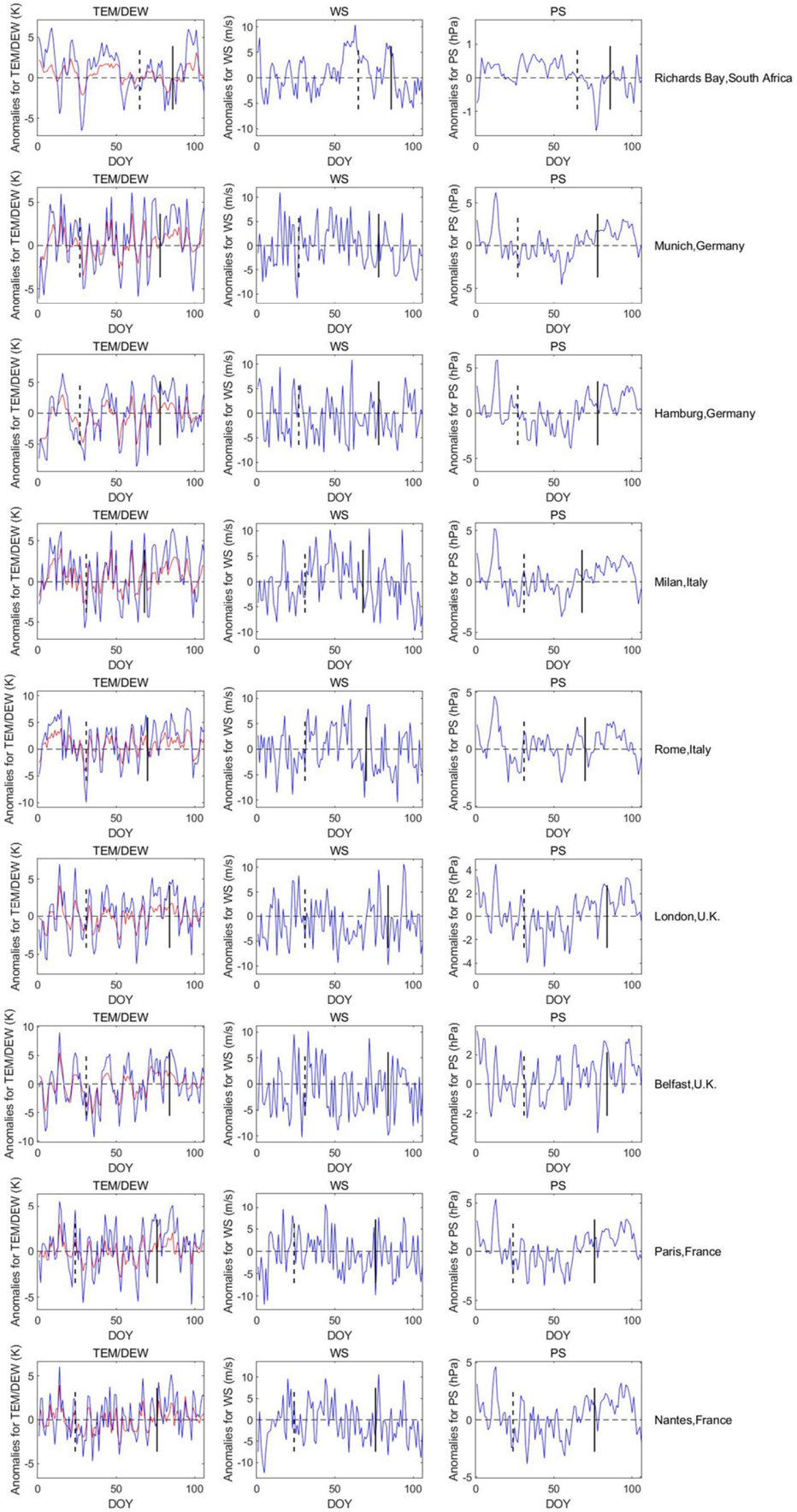


752
753 **Figure S13(2).** The daily variations of meteorological anomalies in 2020 in the 26 cities—part 2.

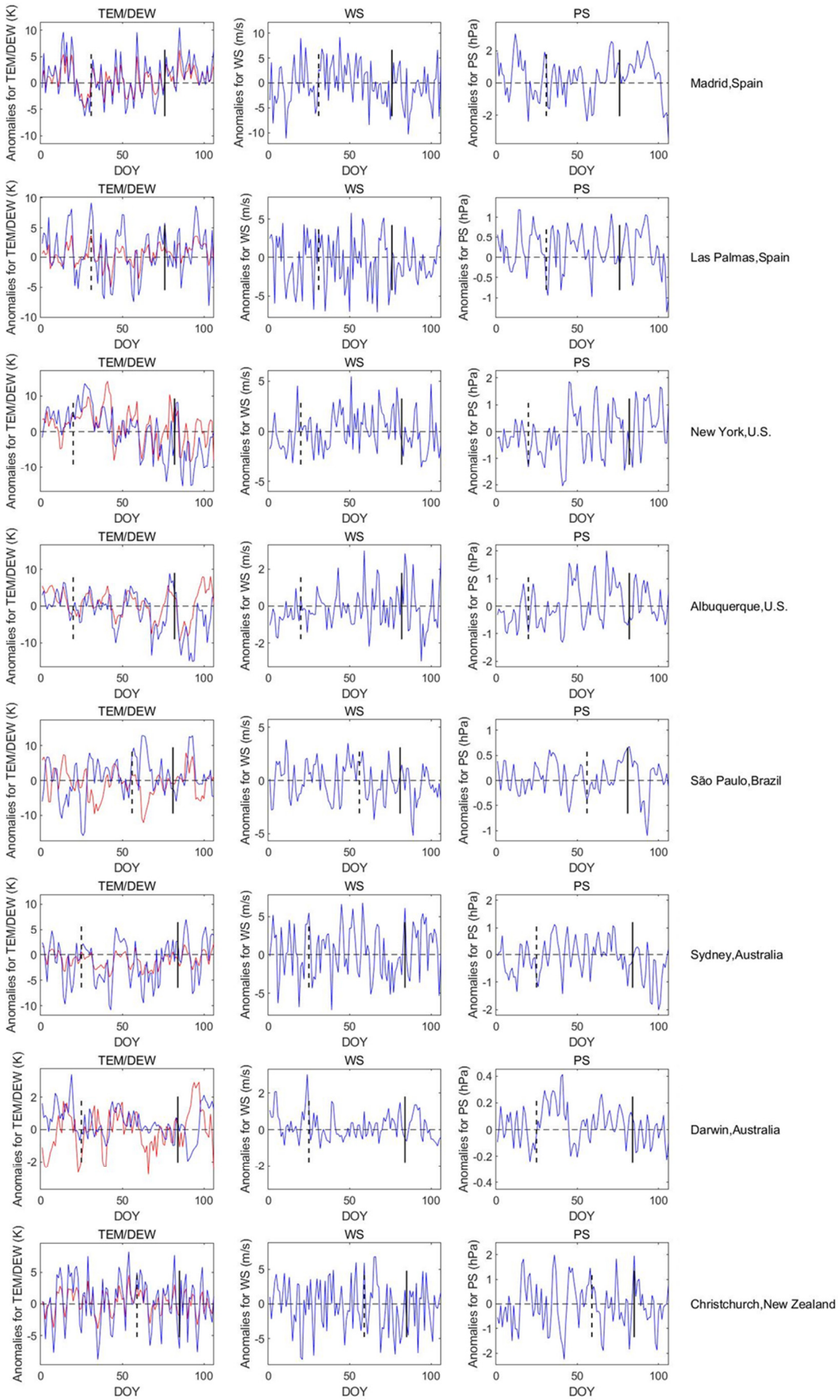


754
755 **Figure S13(3).** The daily variations of meteorological anomalies in 2020 in the 26 cities—part 3.
756

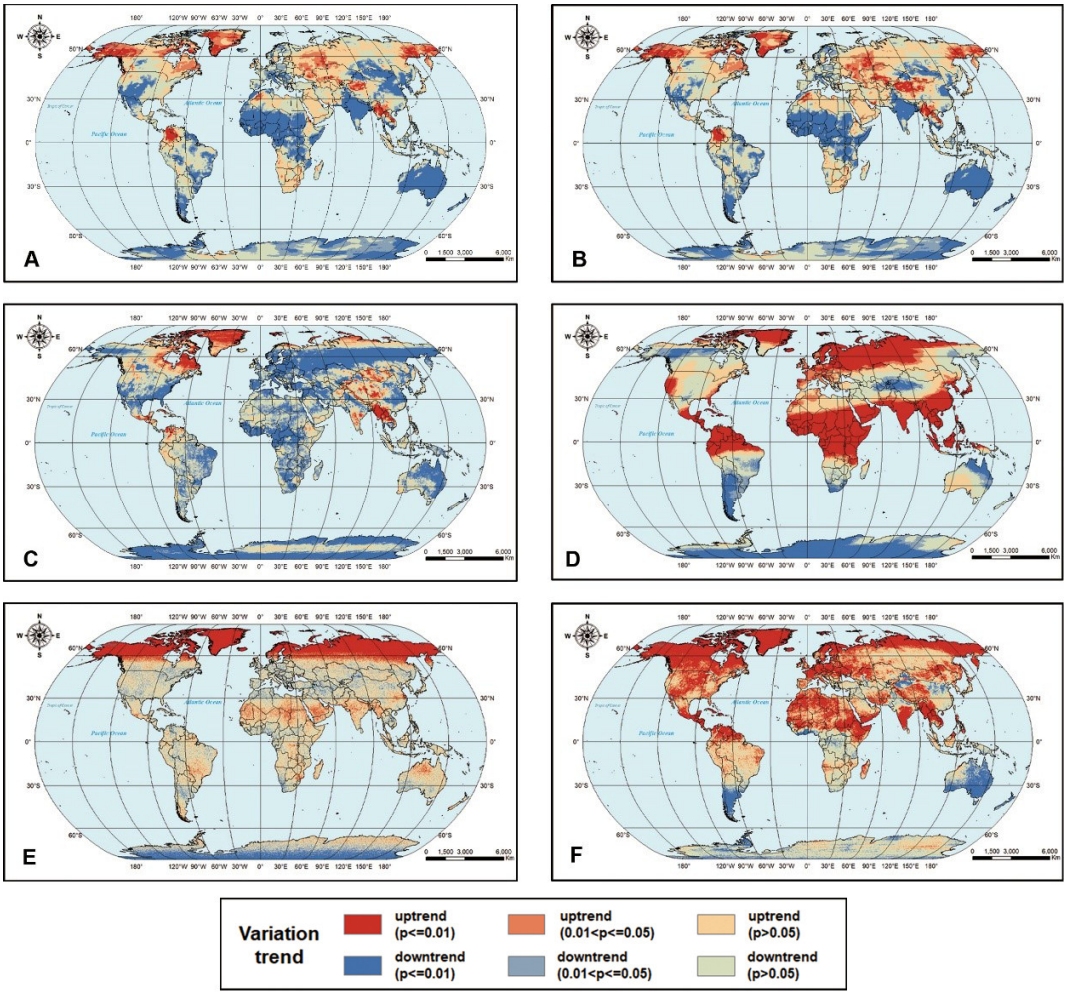


**Figure S14.** Global variation trends and significances of six pollutants during COVID-19. (A-L) represents variation trends and significances of original observations of $PM_{2.5}$, $PM_{10}$, $NO_2$, $O_3$, $SO_2$, and CO, respectively. All results were calculated by MK test.

# Supplemental Tables

**Table S1.** The percent of AQI change after FCC/lockdown (per1/per2) for six pollutants in 26 cities. Cities above the dashed line are quick-response cities, and cities below the dashed line are slow-response cities.

| City | $PM_{2.5}$ | | $PM_{10}$ | | $SO_2$ | | $NO_2$ | | $O_3$ | | CO | |
|---|---|---|---|---|---|---|---|---|---|---|---|---|
| | per1 | per2 | per1 | per2 | per1 | per2 | per1 | per2 | per1 | per2 | per1 | per2 |
| Richards Bay | NaN | -79.07% | 25.72% | -21.65% | 9.23% | 1.28% | NaN | -58.36% | NaN | 25.65% | NaN | NaN |
| Wuhan | NaN | -6.44% | NaN | -7.63% | NaN | 2.91% | NaN | -36.35% | NaN | 83.92% | NaN | 20.73% |
| Xining | NaN | -22.19% | NaN | -61.64% | NaN | 15.58% | NaN | -16.87% | NaN | -3.53% | NaN | -15.43% |
| São Paulo | 4.13% | -3.40% | 14.42% | -14.83% | 4.46% | -37.84% | -4.81% | -23.67% | 26.15% | 13.32% | -28.90% | 0.39% |
| Christchurch | -4.88% | -1.13% | 12.84% | -13.66% | 110.01% | 290.37% | -32.54% | -75.10% | NaN | NaN | -7.24% | 29.93% |
| Tehran | 20.14% | -18.52% | 4.74% | -9.46% | -8.10% | -7.06% | -9.49% | -11.58% | NaN | NaN | 18.97% | 16.86% |
| Daegu | 5.79% | -19.76% | -1.18% | -4.37% | -4.03% | 6.88% | 2.00% | -22.56% | -13.69% | 3.51% | 4.40% | -26.76% |
| Milan | -21.94% | 6.28% | -25.42% | 9.98% | -2.33% | -16.30% | -12.64% | -16.90% | 131.56% | -11.74% | NaN | NaN |
| Rome | -30.98% | 15.04% | -34.07% | 5.36% | -10.73% | 36.06% | -13.72% | -32.85% | 58.05% | 0.18% | NaN | NaN |
| Madrid | 0.82% | -19.22% | -6.24% | -27.96% | -0.99% | -1.41% | 1.92% | -31.10% | -29.79% | 10.49% | NaN | NaN |
| Las Palmas | 53.67% | -43.06% | 80.83% | -55.17% | 0.10% | 15.57% | 16.55% | -31.78% | -8.03% | -9.05% | NaN | NaN |
| Munich | NaN | NaN | -44.87% | 128.57% | NaN | NaN | -44.66% | -1.43% | 112.43% | 1.30% | NaN | NaN |
| Hamburg | -55.32% | 46.22% | -55.25% | 52.00% | 10.76% | 20.77% | -17.40% | 3.69% | 23.69% | -11.82% | NaN | NaN |
| Paris | -18.66% | 54.37% | -12.34% | 30.05% | -7.03% | 39.55% | -32.95% | -14.54% | 38.12% | -6.38% | -30.60% | 212.88% |
| Nantes | 1.17% | 72.18% | -1.79% | 31.19% | NaN | NaN | -20.94% | 4.55% | 2.39% | -13.57% | NaN | NaN |
| London | -16.70% | 48.25% | -15.92% | 43.53% | 17.54% | -10.44% | -0.76% | -7.37% | 23.99% | 13.64% | -2.16% | -14.94% |
| Belfast | -2.90% | -20.81% | -5.61% | -2.04% | 11.44% | -76.57% | -6.11% | -44.68% | -18.22% | 47.18% | 94.54% | -5.47% |
| Mumbai | -0.94% | -4.50% | 10.19% | -10.53% | 62.07% | -29.18% | 6.50% | -57.08% | -3.43% | -0.79% | 15.06% | -22.27% |
| Patna | 0.56% | -12.33% | NaN | NaN | -18.13% | -3.45% | 179.71% | 45.60% | -103.96% | 99.72% | 19.48% | -11.42% |
| Sydney | -57.17% | -13.61% | -43.07% | -12.52% | 18.97% | -7.02% | 3.07% | -6.75% | -10.72% | -7.35% | -49.83% | -18.77% |
| Darwin | -14.32% | -31.23% | 18.69% | -31.15% | 3.95% | -34.88% | -16.85% | 8.95% | 2.65% | -30.21% | 23.27% | -14.09% |
| Yeosu | 0.30% | -19.26% | -13.84% | 0.65% | -8.21% | -12.76% | -4.86% | -19.95% | 2.79% | -12.22% | 4.04% | -16.24% |
| New York | -4.81% | -15.53% | NaN | NaN | NaN | NaN | 1.48% | -37.12% | -1.99% | 1.95% | 7.97% | -35.68% |
| Albuquerque | 28.13% | 3.13% | 23.45% | 5.24% | NaN | NaN | 9.08% | -6.94% | -31.31% | 9.83% | 30.54% | 13.00% |
| Toyko | -24.44% | -19.74% | -31.41% | -34.00% | -9.00% | -18.40% | -2.78% | -11.48% | -7.09% | 10.12% | -2.99% | -3.67% |
| Akita | -9.55% | -32.58% | -48.61% | -72.12% | NaN | NaN | -26.70% | -3.57% | 5.53% | -5.32% | 5.81% | 2.61% |

**Table S2.** Correlation between detected change point in time series and time of first case confirmation and lockdown.

| | | First-case-confirmation time | | Lockdown time | |
|---|---|---|---|---|---|
| | | r | p | r | p |
| All cities | $PM_{2.5}$ | 0.53* | 0.01 | 0.26 | 0.21 |
| | $PM_{10}$ | 0.41* | 0.04 | 0.28 | 0.19 |
| | $SO_2$ | 0.23 | 0.29 | 0.46* | 0.03 |
| | $NO_2$ | 0.69* | 0.00 | 0.58* | 0.00 |
| | $O_3$ | 0.51* | 0.01 | 0.56* | 0.00 |
| | CO | 0.48* | 0.02 | 0.30 | 0.15 |
| Quick response cities | $PM_{2.5}$ | 0.73* | 0.01 | 0.57* | 0.05 |
| | $PM_{10}$ | 0.57* | 0.05 | 0.49 | 0.11 |
| | $SO_2$ | 0.54 | 0.07 | 0.48 | 0.11 |
| | $NO_2$ | 0.92* | 0.00 | 0.91* | 0.00 |
| | $O_3$ | 0.74* | 0.01 | 0.80* | 0.01 |
| | CO | 0.60 | 0.07 | 0.70* | 0.02 |
| Slow response cities | $PM_{2.5}$ | 0.31 | 0.30 | -0.01 | 0.97 |
| | $PM_{10}$ | -0.08 | 0.80 | 0.21 | 0.51 |
| | $SO_2$ | -0.38 | 0.25 | 0.09 | 0.79 |
| | $NO_2$ | 0.37 | 0.19 | -0.01 | 0.97 |
| | $O_3$ | -0.20 | 0.49 | 0.41 | 0.15 |
| | CO | 0.58* | 0.03 | -0.38 | 0.18 |

Note: * represents the correlation coefficient is significant at 95% significance level.

**Table S3.** Percent of AQI anomalies change in different continents. $per_1$ represent the percent of change after first case confirmation before lockdown; $per_2$ represent the percent of change after lockdown.

| | **$PM_{2.5}$** | | **$PM_{10}$** | | **$NO_2$** | |
|---|---|---|---|---|---|---|
| | $per_1$ | $per_2$ | $per_1$ | $per_2$ | $per_1$ | $per_2$ |
| **Asian & Africa** | -1% (-11%, 8%) | -23% (-36%, -11%) | -8% (-25%, 10%) | -25% (-41%, -8%) | -6% (-14%, 3%) | -26% (-39%, -14%) |
| **Europe** | -18% (-30%, -6%) | 25% (3%, 48%) | -22% (-34%, -11%) | 30% (3%, 57%) | -16% (-26%, -7%) | -16% (-26%, -5%) |
| **Other regions** | -8% (-29%, 12%) | -10% (-19%, -1%) | 5% (-16%, 27%) | -13% (-23%, -3%) | -7% (-18%, 4%) | -23% (-45%, -2%) |
| **All cities** | -7% (-17%, 3%) | -5% (-18%, 7%) | -7% (-19%, 6%) | -3% (-19%, 13%) | -9% (-16%, -3%) | -22% (-30%, -14%) |
| | **$O_3$** | | **$SO_2$** | | **CO** | |
| | $per_1$ | $per_2$ | $per_1$ | $per_2$ | $per_1$ | $per_2$ |
| **Asian & Africa** | -20% (-50%, 10%) | 22% (-3%, 48%) | 3% (-15%, 22%) | -5% (-13%, 4%) | 9% (3%, 15%) | -6% (-16%, 4%) |
| **Europe** | 38% (4%, 72%) | 3% (-9%, 15%) | 3% (-5%, 10%) | -1% (-29%, 26%) | 21% (-40%, 81%) | 64% (-55%, 183%) |
| **Other regions** | -3% (-19%, 13%) | -2% (-16%, 11%) | 9% (-1%, 17%) | -27% (-42%, -11%) | -4% (-27%, 19%) | -4% (-21%, 13%) |
| **All cities** | 9% (-11%, 30%) | 9% (-3%, 20%) | 4% (-4%, 12%) | -6% (-17%, 6%) | 6% (-9%, 21%) | 6% (-18%, 31%) |

*Numbers in the brackets represent the 95% confidence intervals. The negative sign indicates a decrease and the positive sign represent the increase. Patna was removed when calculating the mean percent of change for $NO_2$ in Asia and Africa region, in that the change of $NO_2$ in Patna can be special as described in the main text. For the analysis of $SO_2$ in other regions, Christchurch was removed for the same reason. Other regions include cities in North America, South America and Australia.

782 **Table S4.** Healthy effect of AQI levels.

| AQI | Air Pollution Level | Health Implications | Cautionary Statement (for PM2.5) |
|---|---|---|---|
| 0 - 50 | Good | Air quality is considered satisfactory, and air pollution poses little or no risk | None |
| 51 -100 | Moderate | Air quality is acceptable; however, for some pollutants there may be a moderate health concern for a very small number of people who are unusually sensitive to air pollution. | Active children and adults, and people with respiratory disease, such as asthma, should limit prolonged outdoor exertion. |
| 101-150 | Unhealthy for Sensitive Groups | Members of sensitive groups may experience health effects. The general public is not likely to be affected. | Active children and adults, and people with respiratory disease, such as asthma, should limit prolonged outdoor exertion. |
| 151-200 | Unhealthy | Everyone may begin to experience health effects; members of sensitive groups may experience more serious health effects | Active children and adults, and people with respiratory disease, such as asthma, should avoid prolonged outdoor exertion; everyone else, especially children, should limit prolonged outdoor exertion |
| 201-300 | Very Unhealthy | Health warnings of emergency conditions. The entire population is more likely to be affected. | Active children and adults, and people with respiratory disease, such as asthma, should avoid all outdoor exertion; everyone else, especially children, should limit outdoor exertion. |
| 300+ | Hazardous | Health alert: everyone may experience more serious health effects | Everyone should avoid all outdoor exertion |

783
784

# Supplemental Materials and Method

## Study region for ground-based analysis.

We selected 26 different cities and analyze the Air quality index (AQI) data of six main atmospheric pollutants ($PM_{2.5}$, $PM_{10}$, $NO_2$, $O_3$, $SO_2$, CO) from local environmental monitoring stations. The selected 26 cities included both cities with a large number of infections and a relatively small number of infections, and included both cities with strong lockdown restrictions and soft lockdown restrictions[1], for comprehensive coverage of different types of cities. These cities also covered all the continents besides Antarctica. The lockdown time and the first case confirmation time were collected from online news which reported the COVID-19 pandemic progress in the world. The first case confirmation time refers to the time when the first COVID-19 case was found in the country. The lockdown time refers to the time when the government closes most of the unnecessary public places and requires residents to stay at home unless in a special circumstance or the time when the government claims an emergency.

## Data collection and preprocessing

Ground-based measurements. AQI were used for analysis. AQI aims to evaluate the healthy effect after breathing polluted air for some time (usually 24 hours). For example, the AQI value being 188 (unhealthy) means that if a person stays out for 24 hours, the AQI is 188 during those 24 hours, then the health effect is Unhealthy, which is quite different from that if the AQI reported now is 188, then the health effect is Unhealthy. More information about healthy effect of AQI levels can be found in Table S4. The algorithm that convert raw concentrations to AQIs (scale from 0 to 500) is shown as following Equation.

$$AQI_j = \frac{AQI_{Hi} - AQI_{Lo}}{BP_{Hi} - BP_{Lo}}(C_j - BP_{Lo}) + AQI_{Lo}$$

where $AQI_j$ refers to the AQI for pollutant $j$, including $PM_{2.5}$, $PM_{10}$, $SO_2$, $NO_2$, $O_3$ and CO. $C_j$ refers to the raw concentration of pollutant $j$, $BP_{Hi}$ refers to the higher threshold of concentration $C_j$, $BP_{Lo}$ refers to the lower threshold of concentration $C_j$, $AQI_{Hi}$ refers to the AQI threshold for corresponding $BP_{Hi}$, and $AQI_{Lo}$ refers to the AQI threshold for corresponding $BP_{Lo}$.

As shown, raw concentrations and AQIs can be converted to each other theoretically. However, the raw concentrations usually cannot be calculated inversely from AQIs because the thresholds (i.e. $BP_{Hi}$ and $BP_{Lo}$) varies from country to country and often unavailable. Therefore, we calculated anomalies based on AQIs data uniformly when conducting time series analysis for ground-based data

AQI data for six main atmospheric pollutants from ground monitoring stations[2] was provided by the World Air Quality Index project. The project is providing transparent air quality information for more than 100 countries, covering more than 12,000 stations in 1000 major cities, via the website: https://aqicn.org/. All the Air Quality data seen on World Air Quality Index are the official data from each country's respective Environmental Protection Agency (EPA). The AQI standard for every single published station is based on the US EPA Instant-Cast standard. Quality of the data has been controlled through a set of real-time artificial intelligent (AI) algorithms (detect abnormal data conditions such as sparks, low reporting, etc. and automatically 'disable' data reported from defective stations.). Historical air quality data were provided on the database platform page (https://aqicn.org/data-platform/register/) and real-time air quality data can be accessed using the API (https://aqicn.org/api/). Recently, this website has also published AQI data for cities in the world, and data was given in the form of max value, min value, median, and variance. The median data was used to represent the AQI level in the city in this study. Then data for the 26 selected cities were extracted. The study period of ground station measurements was from 1 January to 24 April 2020.

We deleted abnormal values (such as zero value, negative value, etc.) in the original time series data. After data quality check and filtering, for most of the 26 selected cities, there were six kinds of pollutants available, and for other cities, data for some kinds of pollutants are missing. We listed cities which the data are lacked for each kind of pollutant below:

- $PM_{2.5}$: Munich
- $PM_{10}$: Patna, New York
- $NO_2$: \
- $O_3$: Tehran, Christchurch
- $SO_2$: Akita, Munich, Nantes, New York
- CO: Christchurch, Munich, Hamburg, Milan, Rome, Nantes, Madrid, Las Palmas

Satellite observations and reanalysis data. The study period of satellite observations and reanalysis data was from 1 January to 31 March 2020. The concentration data for four kinds of gas pollutants ($NO_2$, $O_3$, $SO_2$, CO) were obtained from TROPOspheric Monitoring Instrument (TROPOMI) and Ozone Monitoring Instrument (OMI); the $PM_{2.5}$ and $PM_{10}$ ($PM_x$) concentration data were provided by the Copernicus Atmosphere Monitoring Service (CAMS) reanalysis data.

The Sentinel-5 Precursor (Sentinel-5P) satellite mission is one of the European Space Agency's (ESA) new mission family: Sentinels. The sensor payload on Sentinel-5P is TROPOMI[3], which is a nadir-viewing 108° Field-of-View push-broom grating hyperspectral spectrometer, covering the wavelength of Ultraviolet-Visible (UV), Near Infrared (NIR), and ShortWave InfraRed (SWIR). Sentinel-5P is the first of the atmospheric composition sentinels and is expected to provide measurements of $O_3$, $NO_2$, $SO_2$, etc. at high spatial, temporal, and spectral resolutions. In our study, TROPOMI products of $NO_2$, $SO_2$, CO, and $O_3$ in 2020 and 2019 are employed. The CO product has a spatial resolution of 0.07°×0.0.7°, while that of other products utilized is 0.05°×0.05°. All products have the same temporal resolution of daily and were resampled to 0.1°×0.1° using the bilinear interpolation.

OMI[4] employs hyperspectral imaging in a push-broom mode to observe solar backscatter radiation in the visible and UV bands, which is onboard the Aura satellite. The Earth will be viewed in 740 wavelength bands along the satellite track with a swath large enough to provide global coverage in 14 orbits (1-day). OMI will continue the Total Ozone Mapping Spectrometer (TOMS) record for $O_3$ and other atmospheric parameters related to $O_3$ chemistry and climate, including $NO_2$, formaldehyde (HCHO), and aerosol characteristics. In our study, OMI products of $NO_2$ and $O_3$, whose spatial resolution are 0.25°×0.25° and temporal resolution are daily, in 2017 and 2018 are collected and resampled to 0.1°×0.1° using the bilinear interpolation. The units for all the satellite data are unified into DU.

CAMS reanalysis[5] is the latest global reanalysis dataset of atmospheric composition, including aerosols and atmospheric chemical species. The dataset builds on the experience gained during the production of the earlier Monitoring Atmospheric Composition and Climate (MACC) reanalysis and CAMS interim reanalysis. CAMS reanalysis can provide surface-level products of atmospheric compositions (e.g. $NO_2$ and $PM_x$) at a high temporal resolution (3-hour) but relatively low spatial resolution (0.8°×0.8°), which are gridded data sets constructed by blending satellite observations with model simulations. In our study, CAMS products of $PM_{2.5}$ and $PM_{10}$ are utilized and resampled to 0.1°×0.1° using the bilinear interpolation and averaged to daily.

The global meteorological data were also provided by CAMS, with a 3-hour and 0.4°x0.4° resolution. We selected 6 commonly used meteorological variables for analysis, including: temperature (full name in the product: 2m temperature, abbreviation in the manuscript: TEM), dewpoint temperature (2m dewpoint temperature, DEW), zonal wind (10m u-component of wind,

UWS), meridional wind (10m v-component of wind, VWS), precipitation (large-scale precipitation, PRE), and pressure (mean sea-level pressure, PS). The 3-h data was averaged to the daily data for analysis in this study. When analyzing the meteorological conditions for specific city, the pixels within the bounding rectangle of the city's administrative boundary were averaged to represent the meteorological condition of the city. The anomalies and the change of meteorological factor in different periods were calculated using the same method as the ground based AQI data. The composite wind speed was calculated from the zonal wind speed and meridional wind speed using the following equation:

$$WS = \sqrt{UWS^2 + VWS^2} .$$

Transportation data include two parts. For Chinese cities, the intra-city travel intensity data from the Baidu map (http://qianxi.baidu.com) was used, which can be accessed through the Application Program Interface (API) provided by Baidu. Intra-city travel intensity represents the indexed result of the ratio of the number of people traveling in the city to the city 's inhabitants, and the data is available from 1 January to 24 April 2020.

For other cities in the world, the transportation data was provided by Google Community Mobility Reports (https://www.google.com/covid19/mobility/), which are aimed to provide insights into what has changed in response to policies aimed at combating COVID-19 aim. The reports chart movement trends over time by geography, across different categories of places such as retail and recreation, groceries and pharmacies, parks, transit stations, workplaces, and residential. These categories are divided based on google map and the movement trends are collected by google accounts' location history data anonymously. Changes for each day are compared to a baseline value for that day of the week. The baseline is the median value, for the corresponding day of the week, during a 5-week period of 3 January to 6 February 2020. The data were provided for different regions in the world with varying spatial scales. For example, for Korea, the data were provided in the unit of the country, that's to say, there is only one data for one day in the country. For Italy, the data were provided in the unit of Region, such as Lombardia and Lazio. For Japan, the data were provided in the unit of the city, such as Tokyo and Akita. Overall, for most areas, the data were provided in the unit of first-level administrative division in each country. Since we mainly studied the air quality change in city-scale when analyzing the ground-based data, the Google mobility data were also matched with our selected 26 cities. We represent the mobility in the city using mobility data of the region where it belongs. The data was accessible since 15 February 2020. Since start date can be later than the time of the first case confirmation in most countries, when calculating the contribution of the first case confirmation and lockdown to the mobility data decrease, we utilized the first case confirmation time of local region rather than of the whole country.

**Processing of missing data**

We usually calculated averaged measurements of previous three years as baseline when conducting time series analysis for satellite and reanalysis data. But for SO2 and CO data, only data from 2019 were used to calculate anomalies for the lack of data in 2017 and 2018.

Ground-based dataset also has missing part. For Tehran, Iran, data of 2017 was lacking, and only data in 2018 and 2019 were used as baseline; for PM2.5, NO2 and O3 AQI data in Richards Bay, South Africa, data in 2017 and 2018 were lacking, and only data in 2019 were used as a baseline.

## Supplemental References


1. COVID-19 pandemic by country and territory in Wikipedia https://en.wikipedia.org/wiki/COVID-19_pandemic_by_country_and_territory [accessed 18 May 2020]
2. Wang, Y., Ying, Q., Hu, J., and Zhang, H. (2014). Spatial and temporal variations of six criteria air pollutants in 31 provincial capital cities in China during 2013–2014. Environ. Int. 73, 413–422.
3. Veefkind, J.P., Aben, I., McMullan, K., Förster, H., de Vries, J., Otter, G., Claas, J., Eskes, H.J., de Haan, J.F., Kleipool, Q., et al. (2012). TROPOMI on the ESA Sentinel-5 Precursor: A GMES mission for global observations of the atmospheric composition for climate, air quality and ozone layer applications. Remote Sens. Environ. *120*, 70–83.
4. Levelt, P.F., Oord, G.H.J. van den, Dobber, M.R., Malkki, A., Visser, H., Vries, J. de, Stammes, P., Lundell, J.O. V, and Saari, H. (2006). The ozone monitoring instrument. IEEE Trans. Geosci. Remote Sens. *44*, 1093–1101.
5. Inness, A., Ades, M., Agustí-Panareda, A., Barré, J., Benedictow, A., Blechschmidt, A.-M., Dominguez, J.J., Engelen, R., Eskes, H., Flemming, J., et al. (2019). The CAMS reanalysis of atmospheric composition. Atmos. Chem. Phys. *19*, 3515–3556.